K27-linked diubiquitin inhibits UCHL3 via an unusual kinetic trap

Tilburg, G.B.A. van; Murachelli, A.G.; Fish, A.; Noort, G.J.V. van; Ovaa, H.; Sixma, T.K.

Cell Chemical Biology

CellPress

Article

K27-Linked Diubiquitin Inhibits UCHL3 via an Unusual Kinetic Trap

Gabriëlle B.A. van Tilburg,[1,4] Andrea G. Murachelli,[2,4] Alexander Fish,[2] Gerbrand J. van der Heden van Noort,[1,*] Huib Ovaa,[1,3] and Titia K. Sixma[2,5,*]

[1]Department of Cell and Chemical Biology and Oncode Institute, Leiden University Medical Center, Einthovenweg 20, 2333 ZC Leiden, the Netherlands

[2]Department of Biochemistry and Oncode Institute, Netherlands Cancer Institute, Plesmanlaan 121, 1066 CX Amsterdam, the Netherlands

[3]In memory of Huib Ovaa, who died too early on May 19, 2020. His curiosity and passion for science will always be an example

[4]These authors contributed equally

[5]Lead Contact

*Correspondence: gvanderheden@lumc.nl (G.J.v.d.H.v.N.), t.sixma@nki.nl (T.K.S.)

https://doi.org/10.1016/j.chembiol.2020.11.005

SUMMARY

Functional analysis of lysine 27-linked ubiquitin chains (^{K27}Ub) is difficult due to the inability to make them through enzymatic methods and due to a lack of model tools and substrates. Here we generate a series of ubiquitin (Ub) tools to study how the deubiquitinase UCHL3 responds to ^{K27}Ub chains in comparison to lysine 63-linked chains and mono-Ub. From a crystal structure of a complex between UCHL3 and synthetic $^{K27}Ub_2$, we unexpectedly discover that free $^{K27}Ub_2$ and $^{K27}Ub_2$-conjugated substrates are natural inhibitors of UCHL3. Using our Ub tools to profile UCHL3's activity, we generate a quantitative kinetic model of the inhibitory mechanism and we find that $^{K27}Ub_2$ can inhibit UCHL3 covalently, by binding to its catalytic cysteine, and allosterically, by locking its catalytic loop tightly in place. Based on this inhibition mechanism, we propose that UCHL3 and ^{K27}Ub chains likely sense and regulate each other in cells.

INTRODUCTION

Ubiquitination is the addition of ubiquitin (Ub) to a lysine or to the initial methionine of a substrate protein. Because Ub itself contains seven lysines and its initial methionine, various Ub chain types can be constructed on the substrate, which translate to different cellular responses (reviewed in Akutsu et al., 2016; Komander and Rape, 2012). Different chain types require specific enzymes for creating, editing, and removing, and are "read" by specific adaptors/effectors. Enzymes responsible for the removal of Ub are called deubiquitinating enzymes (DUBs).

So far, lysine-27-linked Ub chains (K27 chains) have been relatively less studied, due to a lack of enzymatic tools *in vitro*. Only recently reports have emerged that place K27 chains mainly in the intracellular innate immune response pathway, where they regulate several essential infection sensors, such as STING, cGAS, MAVS, and MDA5, or effectors such as NEMO and Beclin. K27-linked chains have also been implicated in the DNA damage repair response (reviewed in Akutsu et al., 2016; van Huizen and Kikkert, 2020).

Previously, we identified ubiquitin carboxyl-terminal hydrolase isozyme 3 (UCHL3) as a tight interactor of lysine-27-linked diubiquitin ($^{K27}Ub_2$) (Zhang et al., 2017). UCHL3 is a DUB belonging to the UCH (ubiquitin carboxy-terminal hydrolase) family, together with UCHL1, UCHL5, and BAP1. UCH family DUBs use a catalytic cysteine as an active nucleophile to attack the (iso)peptide bond between the C-terminal glycine of Ub and the ε-amino or α-amino group of the substrate lysine or methionine. This leads to the formation of a covalent DUB∼Ub thioester intermediate, which is then resolved with a second nucleophilic attack by a water molecule, leading to the release of the substrate (Figure S1A) (Mevissen and Komander, 2017).

To access the catalytic site of UCH DUBs, the ubiquitinated substrate needs to thread underneath a crossover loop (Johnston et al., 1999; Mevissen and Komander, 2017; Misaghi et al., 2005), which closes on top of the C terminus of the conjugated Ub. After catalysis, the loop needs to open again to release the cleaved Ub. The crossover loop of UCHL3 is very short, leading to a specificity for small, preferentially disordered ubiquitinated substrates (Bett et al., 2015; Misaghi et al., 2005; Navarro et al., 2014; Popp et al., 2009; Zhou et al., 2012). *In vivo* substrates of UCHL3 include the precursor of NEDD8 (Hemelaar et al., 2004; Wada et al., 1998), the ribosomal proteins L40 and RPS27a (Grou et al., 2015; Larsen et al., 1998) (both expressed as N-terminal Ub fusions), and the pathological Ub frameshift mutant UBB+1 (Dennissen et al., 2011).

Functionally, UCHL3 has been implicated in DNA damage repair (Liao et al., 2018; Luo et al., 2016; Nishi et al., 2018), regulation of the interferon response (Zhao et al., 2017), meiosis (Mtango et al., 2012), fertilization (Yi et al., 2007), and osteoblast differentiation (Kim et al., 2011). In addition, UCHL3 knockout mice exhibit neuronal, retinal, and muscular degeneration (Semenova et al., 2003), although the mechanistic reasons are unclear. In vertebrates, the closest homolog of UCHL3 is UCHL1

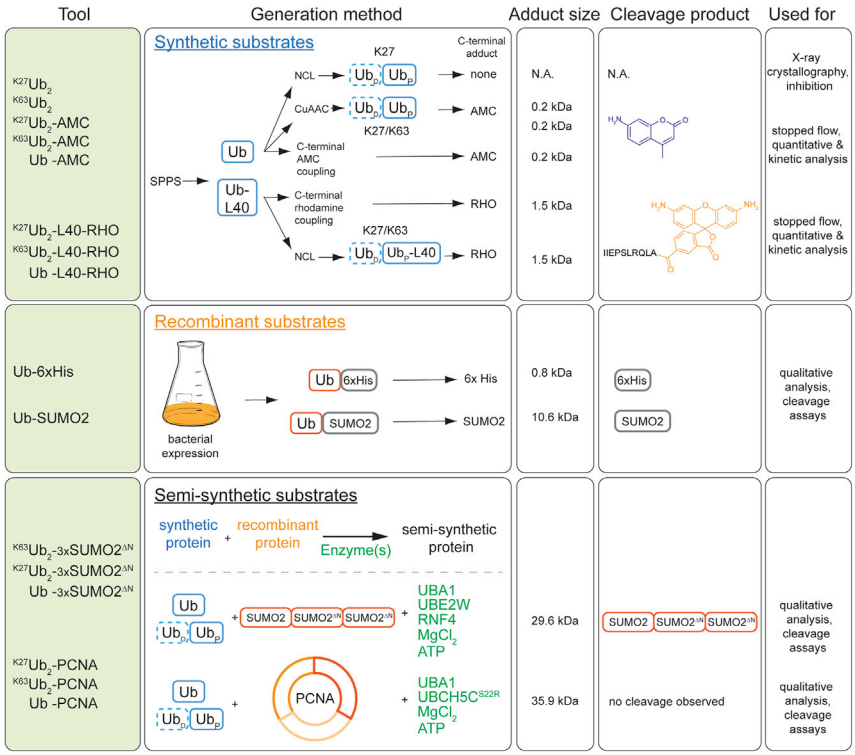

Figure 1. Overview of the Tools Generated to Study the Effect of $^{K27}Ub_2$ Binding to UCHL3

Left to right: (1) designation of each tool; (2) generation method; (3) size of the adduct attached to the C-terminal glycine of Ub/Ub_2 (kilodaltons); (4) products of UCHL3 digestion (Ub/Ub_2 not depicted); (5) assays the tools were used for. SPPS, solid-phase peptide synthesis; AMC, 7-amino-4-methylcoumarin; CuAAC, copper(I)-catalyzed azide-alkyne cycloaddition; L40, ubiquitin-60S ribosomal protein L40-derived peptide (sequence: IIEPSLRQLA); N.A., not applicable; NCL, native chemical ligation; PCNA, proliferating cell nuclear antigen; RHO, rhodamine 110; SUMO2, small ubiquitin-related modifier 2; Ub_D, distal ubiquitin moiety; Ub_P, proximal ubiquitin moiety.

(53% identity in humans), which has overlapping functions in Ub and NEDD8 processing (Hemelaar et al., 2004). Mouse knockout studies suggest that UCHL1 and UCHL3 might have partially overlapping functions in the nervous system (Kurihara, 2001).

In this article, we generate a set of dedicated Ub tools and substrates to study how $^{K27}Ub_2$ binding affects UCHL3 activity. We find that $^{K27}Ub_2$-conjugated substrates potently inhibit UCHL3 activity. Through kinetic analysis followed by global fitting we elucidate the mechanism whereby, surprisingly, $^{K27}Ub_2$ inhibits UCHL3 via a kinetic trap. This is ruled by stochastic events: when UCHL3 binds $^{K27}Ub_2$-conjugated substrates, it can either rapidly cleave and release the hydrolyzed products or be conformationally trapped into a long-lived inhibited state bound to $^{K27}Ub_2$. We predict that if $^{K27}Ub_2$ substrates are in excess, the majority of the UCHL3 population will be trapped into a long-lived inhibited state. This mechanism is specific for UCHL3 and not UCHL1. Finally, the high affinity of UCHL3 for $^{K27}Ub_2$ opens up the possibility of using UCHL3 as a low-cost and easily obtained high-affinity reagent for the detection of free K27 chains.

RESULTS AND DISCUSSION

UCHL3 is one of the few known cellular proteins that bind tightly and specifically to the poorly studied $^{K27}Ub_2$ (Zhang et al., 2017), but how this affects UCHL3 function is not known. Here we used a combination of chemical synthesis, semi-synthesis, genetics, and enzymatic reactions to produce a series of Ub tools that allow mechanistic insights into UCHL3 activities (Figure 1) and quantitative analysis of UCHL3 activity on substrates conjugated to $^{K27}Ub_2$, K63-linked diubiquitin ($^{K63}Ub_2$), or mono-Ub. Because UCHL3 is reported to remove K63-linked tetra-Ub chains from SUMO2 (Bett et al., 2015), we chose to use the K63 linkage as a comparison to the K27 linkage.

UCHL3 Binds to $^{K27}Ub_2$ Selectively, but Does Not Cleave It

First, we quantified the linkage selectivity of UCHL3 for $^{K27}Ub_2$, $^{K63}Ub_2$, and mono-Ub using surface plasmon resonance (SPR) (Figures 2A and 2B). We obtained a dissociation constant (K_d) of 0.046 ± 0.005 μM for $^{K27}Ub_2$, indicating approximately 100-fold preference over $^{K63}Ub_2$ (3.4 ± 0.45 μM) or mono-Ub (5.2 ± 0.3 μM). In contrast, UCHL1, the closest paralog of UCHL3 (53% identity, Figure S2), displays no linkage preference and binds mono-Ub, $^{K27}Ub_2$, and $^{K63}Ub_2$ with similar affinities (1–5 μM, Figures 2A and 2B).

It is known that UCHL3 cannot cleave any of the diubiquitin chains, regardless of the linkage type (Navarro et al., 2014; Popp et al., 2009; Zhou et al., 2012). We confirmed this for $^{K27}Ub_2$ and $^{K63}Ub_2$: at a very high concentration of DUB (4.5 μM) and long incubation times, no significant cleavage was observed (Figure 2C). Apparently UCHL3 binds, but does not cleave, $^{K27}Ub_2$. Remarkably, however, incubation of UCHL3 with $^{K27}Ub_2$ leads to the appearance of a denaturation-resistant band, which corresponds in size to a UCHL3:$^{K27}Ub_2$ complex (marked with * in Figure 2C).

UCHL3 Forms a Thioester Intermediate with $^{K27}Ub_2$ in Crystals

To understand the functional consequence of $^{K27}Ub_2$ binding to UCHL3, we solved a crystal structure of the complex (Figure 3A and Table S1). Our structure closely resembles a previously reported UCHL3:$^{K27}Ub_2$ complex (Pan et al., 2019) (root-mean-square deviation [RMSD] 0.45 Å on 378 Cα), with the exception that our $^{K27}Ub_2$ contains the native isopeptide linkage at the K27 conjugation site, whereas the other structure contains a closely related K27 mimic (Lym27). With different crystallization conditions and packing, our structure independently confirms the relevance of the $^{K27}Ub_2$:UCHL3 binding.

Surprisingly, despite the fact that we used wild-type, native $^{K27}Ub_2$ with a free carboxylic acid on the C terminus (Figure S3A),

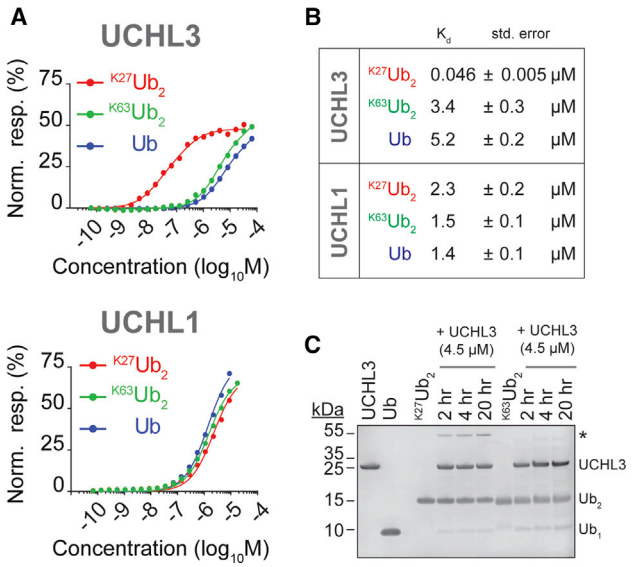

Figure 2. UCHL3 Binds to $^{K27}Ub_2$ Specifically, but Does Not Cleave It

(A and B) (A) Affinity of UCHL3 and UCHL1 for mono-Ub (blue), $^{K27}Ub_2$ (red), and $^{K63}Ub_2$ (green) measured by SPR. All ligands are N-terminally biotinylated. The binding response was normalized for immobilization and molecular weight (see STAR Methods). The data were fitted using a single-site binding model. Norm. resp., normalized response. (B) Dissociation constants from (A). Std. error, standard error.

(C) UCHL3 does not cleave Ub_2. UCHL3 (4.5 μM) and $^{K27}Ub_2$ or $^{K63}Ub_2$ (1 μg) were incubated at 37°C and the time course was resolved by denaturing SDS-PAGE + Coomassie blue staining (5 mM DTT in loading buffer). UCHL3 cannot significantly cleave either Ub_2 linkage. * indicates a denaturation-resistant band whose molecular weight corresponds to the sum of UCHL3 + Ub_2.

the complex crystallized in the shape of the Ub∼DUB thioester intermediate expected during UCH catalysis (Figure S1). The Ub moiety of $^{K27}Ub_2$ that would be attached to a substrate (proximal Ub [Ub_P], Komander and Rape, 2012) occupies the active site of UCHL3 and is linked to UCHL3's catalytic cysteine via continuous electron density, which indicates a thioester bond (Figure 3B). A similar continuous electron density is also observed in the structure of Pan et al. (2019), although the authors did not model a covalent bond (Figure S3C). The interaction between Ub_P and the active site is analogous to the previously reported structure of UCHL3:Ub-vinyl-methyl-ester (Misaghi et al., 2005) (Figure S3B, RMSD 0.63 Å on 303 Cα). The catalytic triad of UCHL3 (Boudreaux et al., 2012; Komander and Rape, 2012) is correctly aligned for catalysis, including the presence of a water molecule required for the second nucleophilic attack (Figure 3B).

UCHL3 Can Form a Thioester Intermediate with $^{K27}Ub_2$ and Mono-Ub under Native Conditions

The observation that UCHL3 can form a stable complex with $^{K27}Ub_2$ under denaturing conditions (Figure 2C) and the occurrence of a thioester bond in our crystal structure prompted us to further investigate the possibility that UCHL3 can form a thioester complex with Ub chains under native conditions. This has been suggested before by Pickart and Rose (Pickart and Rose, 1986). We tested for thioester formation by $NaBH_4$-mediated reduction of mono-Ub or $^{K27}Ub_2$ (58 μM) incubated in presence and absence of UCHL3 (19 μM). A thioester would be reduced to Ub/Ub_2-aldehyde, whereas the free carboxylic acid of Ub/Ub_2 would not (Figure 3C). After 1.5 h incubation at 37°C under mild conditions (Tris-HCl [pH 7.6], 5 mM DTT, 1 mM EDTA), we treated all samples with excess $NaBH_4$. High-resolution mass spectrometry shows the appearance of distinct mass envelopes in the Ub:UCHL3 and $^{K27}Ub_2$:UHCL3 samples that are consistent with the presence of Ub- and $^{K27}Ub_2$-aldehyde, respectively (Figures 3D and 3E), and not Ub- or $^{K27}Ub_2$-alcohol (Figures S3D and S3E). The intensity of both peaks increases with longer $NaBH_4$ incubation (data not shown). The peak observed for $^{K27}Ub_2$-aldehyde is comparably more intense, consistent with the fact that UCHL3 has an ∼100-fold higher affinity for $^{K27}Ub_2$ compared with Ub. Thus, UCHL3 can form covalent thioester bonds with Ub and $^{K27}Ub_2$ in solution under physiological buffer conditions.

The fact that Ub∼UCHL3 and $^{K27}Ub_2$∼UCHL3 thioester complexes can be captured by mass spectrometry and/or crystallization is unexpected, as covalent bond formation between a free carboxyl terminus and a cysteine is energetically disfavored in solution. Indeed, Ub-conjugating enzymes require ATP hydrolysis to form a thioester with Ub in the Ub-conjugation pathway (Komander and Rape, 2012). The influence of mechanical forces on the energy landscape of reactions is widely reported (Bustamante et al., 2004). Upon binding of a proximal Ub, the narrowness of the active channels of UCHL3 seems to disfavor the long-term presence of a free C terminus and active cysteine, pushing toward the formation of a thioester bond. That would suggest that increasing the affinity of Ub_P for the active site, such as is the case for $^{K27}Ub_2$, would promote covalent bond formation.

$^{K27}Ub_2$ Restrains the Crossover Loop of UCHL3

The structure explains the specificity of K27-linkage recognition: the crossover loop of UCHL3 is pinched between the two Ub moieties and adheres to the inner surface created by Ub_P, the side chain of K27, and Ub_D (Figure 4A). This "pinching" of the loop by Ub_2 can occur only with the K27 linkage, since Ub_D in non-K27 Ub_2 would not interact with UCHL3's loop in this manner (Figure S4A). The interaction is mediated by UCHL3 Gln156 protruding toward the K27 linkage and Glu158 engaging in electrostatic interactions with Arg42, Arg72, and Gln49 of Ub_D (Figure 4A). As Glu158 interacts only with Ub_D and not Ub_P, its mutation should affect $^{K27}Ub_2$ binding, but not Ub or $^{K63}Ub_2$. Indeed, UCHL3 E158A and UCHL3 E158R have 10-fold decreased affinity for $^{K27}Ub_2$ relative to wild type, but maintain essentially the same affinity for Ub and $^{K63}Ub_2$ (Figures 4B and 4C).

UCHL1 has 53% sequence identity with UCHL3 (Figure S2), but shows no preference for $^{K27}Ub_2$ (Figures 2A and 2B). The crossover loop in UCHL1 is two residues shorter and it has arginine in the Glu158 position (Figure S2). These differences may prevent UCHL1 from engaging specifically with the distal Ub of $^{K27}Ub_2$. Consequently, these two DUBs must respond differently to ^{K27}Ub in cells.

Free, Unconjugated $^{K27}Ub_2$ Inhibits UCHL3

By pinching the loop, Ub_D prevents it from opening. With a closed loop, Ub_P cannot leave the active site, and the entire $^{K27}Ub_2$ molecule is jammed, so to speak, in the jaws of the

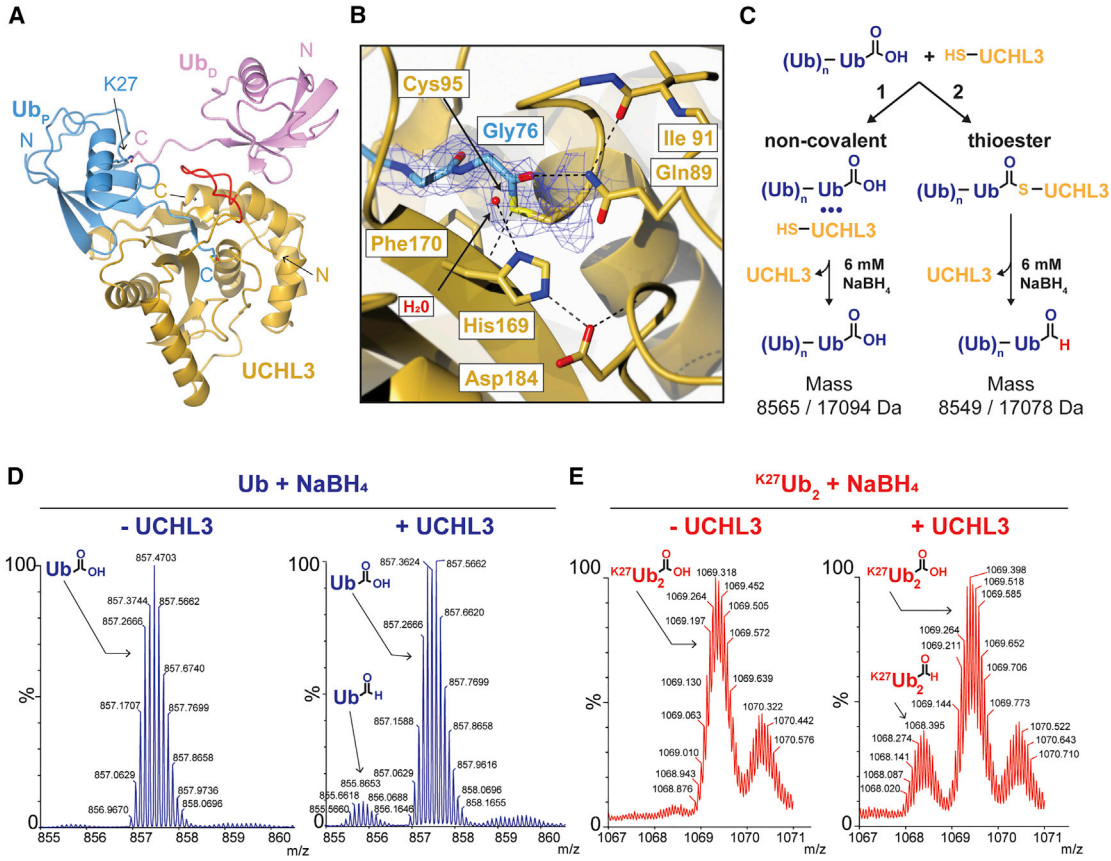

Figure 3. UCHL3 Forms Thioester Bonds with Ub/^{K27}Ub$_2$ in Crystals and in Solution

(A) Structure of UCHL3 in complex with ^{K27}Ub$_2$. The proximal Ub of ^{K27}Ub$_2$ (Ub$_P$, blue) has its C terminus covalently bound to the active site of UCHL3 (gold); the distal Ub (Ub$_P$, pink) sits atop the crossover loop of UCHL3 (red).

(B) UCHL3 forms a thioester bond with ^{K27}Ub$_2$ in crystals. Continuous density (1.5 σ, blue mesh) connects the catalytic cysteine of UCHL3 (gold) to the C terminus of Ub$_P$ (blue). The catalytic triad is aligned and the catalytic water is correctly positioned. Dotted lines, hydrogen bonds.

(C) Expected $NaBH_4$-mediated reduction of a non-covalent (path 1) or a thioester (path 2) UCHL3:Ub$_{(n)}$ complex. Ub aldehyde is formed only with a thioester complex.

(D) UCHL3 forms thioester bonds with Ub in solution. Ub only control or Ub:UCHL3 complex was reduced with excess $NaBH_4$ for 30 min, and the reaction was resolved by mass spectrometry. Sections of the m/z spectra for the Ub only control and Ub:UCHL3 complex are plotted. An extra envelope corresponding to Ub-aldehyde appears when treating the Ub:UCHL3 complex with $NaBH_4$, indicating the presence of a thioester complex (right panel) and no reaction on Ub without UCHL3 present (left panel). The y axis is normalized to the height of the free Ub/Ub$_2$ peak.

(E) As in (D), except that ^{K27}Ub$_2$ was used instead of Ub, and ^{K27}Ub$_2$-aldehyde was detected.

enzyme. This suggests that ^{K27}Ub$_2$ should be an inhibitor of UCHL3. We tested whether mono-Ub or any Ub$_2$ would affect cleavage of the minimal substrate Ub-Rho by UCHL3 (Figure 4D) and found that excess ^{K27}Ub$_2$ results in almost complete inhibition of UCHL3 activity, with effects comparable to those of a covalent inhibitor of cysteine proteases such as iodoacetamide. The other variants showed limited effect that could be due to "product inhibition." This strong inhibitory effect of free ^{K27}Ub$_2$ is also observed when UCHL3 cleaves other substrates such as Ub-His (Figure 4E).

UCHL3 Prefers Smaller Substrates

The structure predicts that UCHL3 could remove K27 chains from substrates, albeit at the likely cost of being inhibited in the process. We compared UCHL3 activity for substrates conjugated to three different Ub types: mono-Ub, ^{K27}Ub$_2$, and ^{K63}Ub$_2$ (Figure 1). It is known that UCHL3 prefers smaller substrates that can easily thread underneath the crossover loop (Bett et al., 2015; Navarro et al., 2014; Popp et al., 2009; Zhou et al., 2012). First, we measured the baseline cleavage speed of UCHL3 against differently sized monoubiquitinated substrates. We incubated comparable amounts of each monoubiquitinated substrate with a range of concentrations of UCHL3 (4.5 pM to 45 μM, in 10-fold increments). In line with previous literature, UCHL3 can swiftly cleave Ub-Rho, readily process Ub-His, or cleave Ub fused to a rhodamine-labeled decapeptide (Ub-L40-Rho, Figure 5A). The L40-decapeptide is derived from a natural substrate of UCHL3, Ub-60S Ribosomal Protein L40 (Grou et al., 2015; Larsen et al., 1998). UCHL3 can also remove a single Ub linearly fused to SUMO2 (Ub-SUMO2, Figures 5A and 5B and Bett et al., 2015) or Ub linearly conjugated to a linear fusion of three SUMO2 molecules (Ub-3×SUMO2$^{\Delta N}$; Bett et al., 2015;

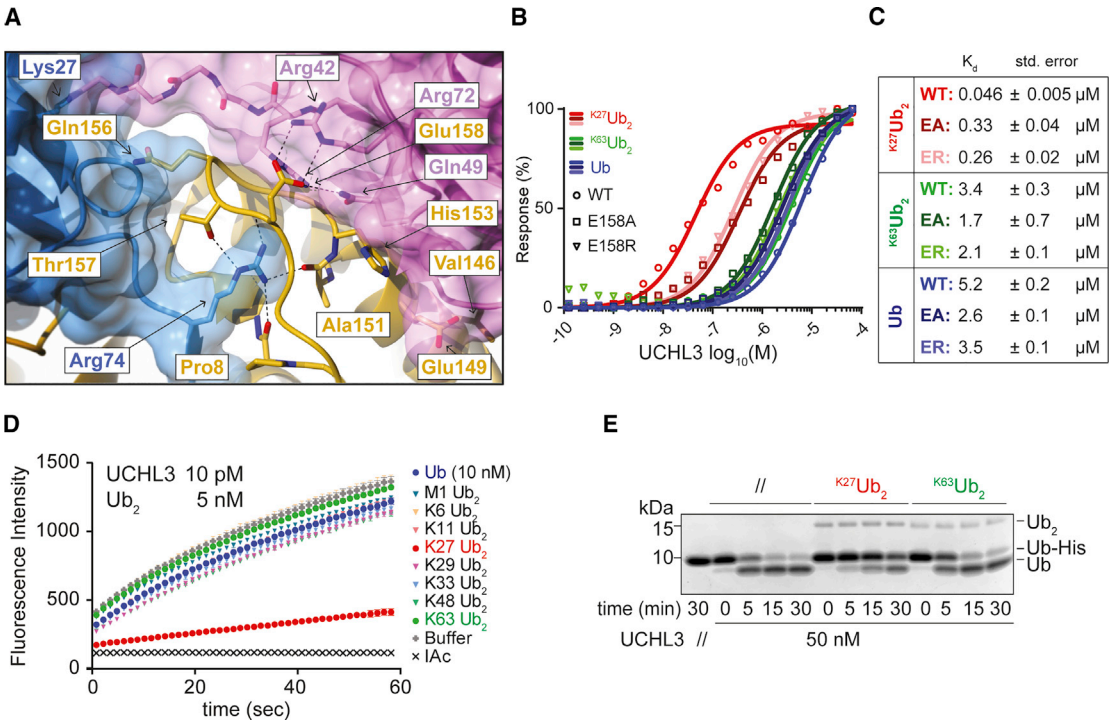

Figure 4. $^{K27}Ub_2$ Inhibits UCHL3

(A) $^{K27}Ub_2$ pinches the crossover loop of UCHL3. Detail of the interaction between the crossover loop of UCHL3 (gold) and the two ubiquitin moieties of $^{K27}Ub_2$ (space fill: Ub_P, blue; Ub_D, pink). The two ubiquitins pinch the crossover loop, and Gln156 of UCHL3 abuts the Lys27 linkage.

(B) Mutations in Glu158 interfere with Ub_D but not Ub_P recognition. SPR measurements of the affinity of mono-Ub (blue), $^{K63}Ub_2$ (green), and $^{K27}Ub_2$ (red) for UCHL3 wild type (WT, circles), UCHL3 E158A (squares), or UCHL3 E158R (triangles). Both mutants bind Ub and $^{K63}Ub_2$ normally, but $^{K27}Ub_2$ more weakly compared with WT.

(C) Dissociation constants from (B).

(D) $^{K27}Ub_2$, but not other diubiquitins, inhibits UCHL3's activity on Ub-Rho. Cleavage of 500 nM Ub-Rho by 0.001 nM UCHL3 was measured in the presence of each Ub_2 at 5 nM or mono-Ub at 10 nM. $^{K27}Ub_2$ strongly inhibits the cleavage reaction. All reactions were measured in quadruplicate and the mean with standard deviation is plotted. IAc, iodoacetamide, covalent inhibitor (negative control).

(E) $^{K27}Ub_2$ inhibits UCHL3's activity on Ub-His. Ub-His (1 μg) and UCHL3 (0.05 nM) were supplemented with 500 nM $^{K27}Ub_2$, $^{K63}Ub_2$, or a buffer control at 37°C. The time course of the digestion was resolved by SDS-PAGE + Coomassie blue staining.

Figure 5C), although the efficiency is much lower than for the smaller substrates, as expected. UCHL3 is, however, unable to remove mono-Ub from the even larger proliferating cell nuclear antigen (PCNA) (Figure 5D). Comparison of cleavage data confirms earlier data: UCHL3 activity decreases with increasing size of the adduct conjugated to the proximal Ub, up to a point where cleavage ceases to happen.

$^{K27}Ub_2$-Conjugated Substrates Inhibit UCHL3 Activity

We then tested how UCHL3 deals with the same substrates when they are conjugated to $^{K27}Ub_2$ or to $^{K63}Ub_2$. We found that UCHL3 could deubiquitinate all substrates, except $^{K27}Ub_2$-PCNA (Figures 5E–5H and data not shown). In line with what we observed in Figure 5A, the cleavage speed of diubiquitinated substrates seemed to generally decrease with increased substrate size, with Ub_2-AMC being fastest, followed by Ub_2-L40-Rho and Ub_2-3×SUMO2$^{\Delta N}$ (compare incubation times in Figures 5E–5H). K27-ubiquitinated substrates were, however, always processed more slowly than their K63-linked counterparts. Thus, as expected, $^{K27}Ub_2$-conjugated substrates inhibit UCHL3 activity. To quantify the inhibition, we used stopped-flow analysis of DUB activity and compared Ub-AMC, $^{K63}Ub_2$-AMC, and $^{K27}Ub_2$-AMC (Figure 5E). $^{K27}Ub_2$-AMC is relatively slower, and, surprisingly, it becomes even slower with increasing substrate-to-enzyme ratio (Figure 5G). In other words, the inhibitory effect of $^{K27}Ub_2$-AMC increases with increasing substrate turnover by the enzyme. This is also the case for Ub/$^{K27}Ub_2$-AMC conjugated to a larger substrate, L40-Rho (Figure 5F).

$^{K27}Ub_2$ Inhibits UCHL3 via a Kinetic Trap

In the experiments presented so far, we showed that the activity of UCHL3 is influenced by the identity of the Ub chain (K27-linked versus non-K27-linked), by the size of the moiety conjugated to the C terminus of the Ub chain, and by whether free $^{K27}Ub_2$ is present. To fully understand the interplay of these three factors and ultimately how $^{K27}Ub_2$ inhibits UCHL3, we used KinTek Explorer (Johnson et al., 2009a) to generate a global kinetic model of UCHL3 cleavage based on the stopped-flow data in Figure 5F and the binding data in Figures 1A and 1B. The cleavage of Ub-AMC and $^{K63}Ub_2$-AMC is fully explained by a simple product inhibition scheme, depicted in the green portion of the model in Figure 6A (see Figure 6B for a table of kinetic constants,

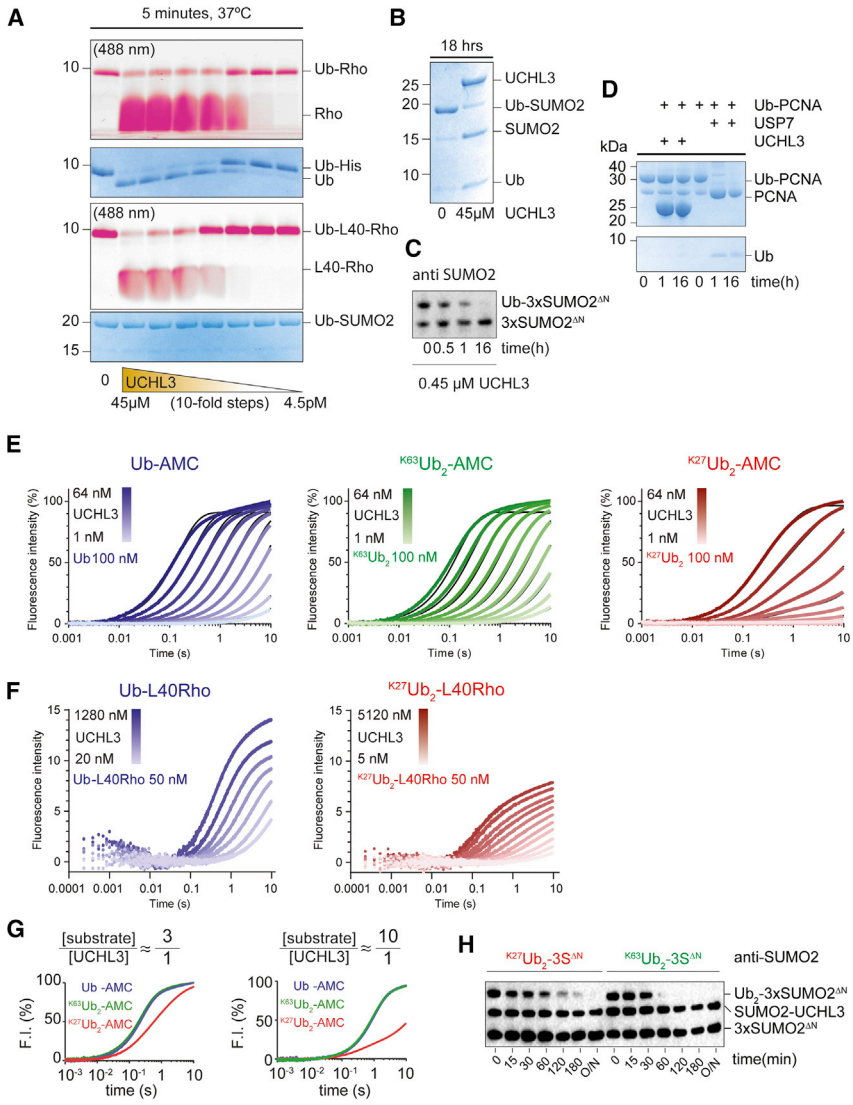

Figure 5. $^{K27}Ub_2$-Conjugated Substrates Inhibit UCHL3 Regardless of Substrate Size

(A–D) UCHL3 cleavage speed decreases with substrate size. (A) One to two micrograms of the indicated substrate was incubated with increasing concentrations of UCHL3 at 37°C for 5 min. The cleavage products were visualized by SDS-PAGE + Coomassie staining (blue) or rhodamine fluorescence (pink). (B) The same amount of Ub-SUMO2 substrate as in (A) was incubated with or without UCHL3 for 18 h. The cleavage reaction was visualized by SDS-PAGE + Coomassie staining. (C) Approximately 0.15 μM Ub-3×SUMO2$^{\Delta N}$ was incubated with 450 nM UCHL3 at 37°C for the indicated times. The cleavage reaction was resolved by western blot (anti-SUMO2). (D) UCHL3 cannot deubiquitinate PCNA. Tri-mono-ubiquitinated PCNA (Ub-PCNA, 0.5 μg) was incubated at 37°C with 45 μM UCHL3 or with 1 μM control DUB (USP7).

(E–G) $^{K27}Ub_2$-conjugated substrates are cleaved more slowly compared with other linkages. (E) Stopped-flow cleavage of Ub-AMC, $^{K63}Ub_2$-AMC, and $^{K27}Ub_2$-AMC. Each substrate (100 nM) was mixed with UCHL3 (0.125–64 nM, in 2-fold increments). The release of AMC results in a fluorescence increase. Black lines show the kinetics predicted from the model in (A). (F) Stopped-flow cleavage of Ub-L40-Rho and $^{K27}Ub_2$-L40-Rho. Same protocol as in (E), but using 50 nM substrate and 20–1,280 nM UCHL3 (Ub-L40-Rho) or 5–5,120 nM UCHL3 ($^{K27}Ub_2$-L40-Rho). (G) $^{K27}Ub_2$-AMC inhibition is stronger for larger excesses of substrate. The reaction curves measured in (E) for each substrate at UCHL3 concentration of 32 nM (substrate:enzyme ratio = 100:32, left) and 8 nM (substrate:enzyme ratio = 100:8, right) were plotted on a common graph. $^{K63}Ub_2$-AMC and Ub-AMC are cleaved faster than $^{K27}Ub_2$-AMC. The inhibitory effect of $^{K27}Ub_2$-AMC is stronger if more catalytic turnovers are required (i.e., at higher substrate:UCHL3 ratios). F.I., fluorescence intensity.

(H) Cleavage of $^{K27}Ub_2$-3×SUMO2$^{\Delta N}$ is slower compared with $^{K63}Ub_2$-3×SUMO$^{\Delta N}$. N-terminally K63- or K27-diubiquitinated 3×SUMO2$^{\Delta N}$ (~0.15 μM) was incubated at 37°C with 45 nM SUMO-tagged UCHL3. The time course was resolved by western blot against SUMO2.

Figure 5F for fit to the data, Figures S5B–S5D for parameter robustness analysis and STAR Methods for details on model fitting). In this model, UCHL3 binds to the $Ub_{(n)}$-AMC substrate, cleaves and releases the fluorophore, and then releases the (di) Ub and is free for further catalysis. Cleaved (di)Ub may compete with unprocessed substrate for binding to the enzyme, resulting in product inhibition. This is the commonly accepted model for UCH-domain DUB catalysis (Mevissen and Komander, 2017) (Figure S1A). A small discrepancy between measurement and prediction in the terminal phase of each reaction (Figure 5E) is likely due to slow cleavage of contaminant misfolded substrate, since this behavior varied between batches. Cleavage of $^{K27}Ub_2$-AMC, however, cannot be fitted by this model. $^{K27}Ub_2$-AMC provides an inhibitory effect that is dependent on the enzyme turnover (Figure 5G), but product inhibition alone could not explain this. The simplest model that captures this effect requires the addition of an extra reaction pathway, shaded in cyan in Figure 6A. According to the complete model, UCHL3 binds to the substrate and then has two possible reaction "choices." One possibility (the "fast track") is the reaction path that is also used for the other Ub chains (green in Figure 6A, estimated probability of this event = 71% ± 13.3%). In this case, the substrate is cleaved, fluorophore and $^{K27}Ub_2$ are released, and the enzyme returns to the active pool. However, there is a second, "slow track," specific for $^{K27}Ub_2$-conjugated substrates (cyan portion of the model in Figure 6B, estimated probability = 29 ± 9.8%). In this path, UCHL3:$^{K27}Ub_2$ must undergo some conformational change before catalysis. Cleavage itself is as fast as in the green path, but after release of the substrate, the reversion of the conformational change to allow release of $^{K27}Ub_2$ is the

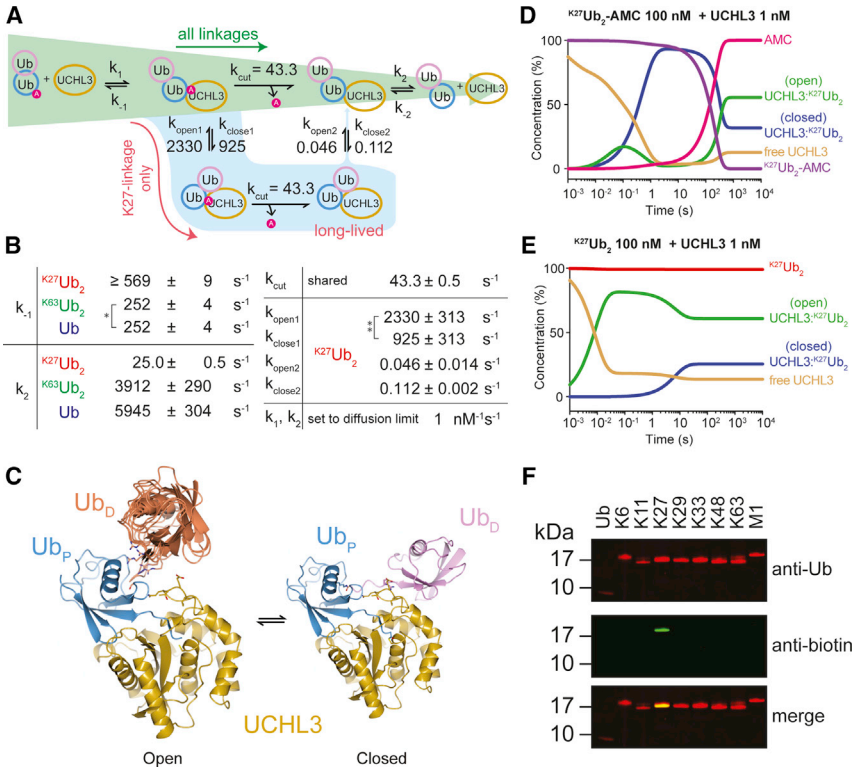

Figure 6. $^{K27}Ub_2$ Inhibits UCHL3 via a Kinetic Trap

(A) Model of the catalytic cycle of UCHL3. The full catalytic model, taking into account allosteric effects of $^{K27}Ub_2$ on UCHL3, is shown. Green, standard (fast) reaction path (all substrates). Cyan, kinetic trap ($^{K27}Ub_2$-conjugated substrates only). A, AMC. Fitting to the raw data is shown in Figure 5E.

(B) Rate constants from (A). *Constrained equal; **linked by constant ratio. k_{-1} for $^{K27}Ub_2$-AMC is determined only as lower bound. k_1 and k_2 have been set to the theoretical solution diffusion limit of 1 nM/s.

(C) Proposed structure and comparison of the open and closed states of the UCHL3: $^{K27}Ub_2$ substrate:DUB complex. The closed conformation is modeled on our crystal structure. The open conformation was modeled by superposing our structure and the NMR structure of free $^{K27}Ub_2$ (PDB: 5UJN; Castaneda et al., 2016) via Ub_P. In several conformations Ub_D (orange) does not touch UCHL3, and the crossover loop can close and allow catalysis. NMR models clashing with UCHL3 are not shown.

(D) $^{K27}Ub_2$ substrates quickly and strongly inhibit UCHL3 activity. Using the model in (A) we simulated a reaction between 1 nM UCHL3 and 100 nM $^{K27}Ub_2$-AMC (100-fold excess substrate). The curves indicate the concentration of each species over time. Within 1 s, UCHL3:$^{K27}Ub_2$ is kinetically trapped, to be released only after minutes following the disappearance of the substrate. Purple, $^{K27}Ub_2$-AMC (substrate); magenta, AMC; gold, free UCHL3; green, open UCHL3:$^{K27}Ub_2$ complex; blue, closed UCHL3:$^{K27}Ub_2$ complex. Time is in log10 scale.

(E) Free $^{K27}Ub_2$ inhibits UCHL3 competitively and allosterically. Analogous to (D), but with 100 nM free $^{K27}Ub_2$ and 1 nM UCHL3. Colors as in (D). Binding of $^{K27}Ub_2$ to UCHL3 induces the appearance of the open complex (product inhibition) and of the closed complex (allosteric inhibition).

(F) UCHL3 can be used as a tool to detect free $^{K27}Ub_2$. Ub and all possible di-Ubs (Lys- and Met-linked) were western blotted using either anti-Ub antibody (mouse) plus IRdye680-conjugated anti-mouse antibody (red, top) or biotinylated UCHL3 C95A plus IRdye800-conjugated neutravidin (green, middle). Bottom: merged signal, showing that UCHL3 recognizes $^{K27}Ub_2$ specifically.

bottleneck of the reaction (Figure 6B, compare the magnitude of k_{open2}/k_{close2} with the other turnover constants). In practice, this means that once UCHL3 takes the slow path, it will be kinetically trapped in a long-lived, stable inhibitory complex with the $^{K27}Ub_2$ product. The probabilistic occurrence of fast and slow pathways explains the observed dependence on catalysis for the inhibition of UCHL3 by $^{K27}Ub_2$-AMC: each round of catalysis increases the cumulative probability that UCHL3 might fall into the inhibitory, kinetic trap.

UCHL3 Activity Is Quickly and Robustly Blocked by Conjugated and Free $^{K27}Ub_2$ Species

We have already shown that K27-ubiquitinated substrates inhibit UCHL3. Our model predicts rapid inhibition. If we simulate a reaction in which 100 nM $^{K27}Ub_2$-AMC substrate is given to 1 nM UCHL3 (Figure 6D), we predict that most of the UCHL3 is inhibited within <1 s of coming into contact with the $^{K27}Ub_2$-AMC substrate. The reaction will then slow down, and UCHL3 will stay >95% inhibited as long as the substrate is present (~15 min in this scenario). If, alternatively, we simulate the addition of 100 nM free and unconjugated $^{K27}Ub_2$ ("product-like") to 1 nM UCHL3, we predict that within 10 s about 80% of the UCHL3 will be inhibited, with 25% of this fraction assuming the long-lived, conformationally inhibited state (Figure 6E). Although the magnitude and speed of inhibition by free $^{K27}Ub_2$ "products" are lower compared with $^{K27}Ub_2$ substrates, in both cases the simulations show that UCHL3 is a sensitive and fast-responding sensor for the presence of $^{K27}Ub_2$ species.

$^{K27}Ub_2$ Inhibition Is Allosteric and Reversibly Covalent

Comparison of UCHL3 structures bound to Ub-vinyl-methyl-ester (Misaghi et al., 2005) and free $^{K27}Ub_2$ (Figure S3B) shows that UCHL3 has not changed, suggesting that inhibitory conformational changes must come from $^{K27}Ub_2$. In the available NMR structures of $^{K27}Ub_2$ in isolation (PDB: 5UJN, Castaneda et al., 2016) there is considerable flexibility between Ub_D and Ub_P (Figure S5C). If we superpose the $^{K27}Ub_2$ NMR ensemble on our structure via Ub_P, there are some conformations of $^{K27}Ub_2$ in which Ub_P can enter the active site without Ub_D making any contact with UCHL3 (Figure 6C, left). These would be compatible with an "open" form of cleavage. To adopt the conformation observed in the crystal structure, Ub_D needs to rotate around its C terminus by about 50°, with Ile44 moving ~25 Å to embrace the crossover loop of UCHL3 (Figure 6C, right). Notably, this conformation of Ub_D is not present in the apo-$^{K27}Ub_2$ NMR ensemble, suggesting that this transition is mediated (or stabilized) by the engagement of UCHL3.

Fluorescence resonance energy transfer measurements of the distance between Ub_P and Ub_D in solution by Pan et al. (Pan et al., 2019) also support this induced-fit model. Overall, the open conformations seem to portray an initial engagement stage, whereas our structure seems to portray a "closed," long-term stable conformation, with the crossover loop locked in place between the two Ub moieties. Based on these structural considerations, we propose that in the kinetic model the "fast track" represents cleavage in the open conformation. Our structure, on the other hand, corresponds to the kinetically trapped reaction intermediate.

Role of the Covalent Bond

Our kinetic model does not explicitly include a covalent thioester bond, and indeed does not require a covalent bond formation step to fit the data well. However, covalent UCHL3:'$^{K27}Ub_2$ complexes exist in solution (Figure 3E) and the model (Figure 6A) does suggest two UCHL3:$^{K27}Ub_2$ complexes coexisting: one with fast exchange rate and one long lived (compare kinetic constants in Figure 6A). It seems likely that the long-lived complex (with a closed $^{K27}Ub_2$ conformation) retains the thioester bond, whereas the open conformation does not. This would explain why $^{K27}Ub_2$-conjugated substrates are better and faster inhibitors than free $^{K27}Ub_2$. $^{K27}Ub_2$-conjugated substrates reach the thioester bond as a natural intermediate in catalysis, and thus can produce the inhibitory complex faster and, at least initially, at higher concentration (compare Figures 6D and 6E). Thus, overall, we speculate that the inhibitory mechanism of $^{K27}Ub_2$ is mediated mainly by the allosteric block of Ub_D on the crossover loop, with a secondary contribution by the covalent binding of Ub_P to the catalytic cysteine.

UCHL3 as a Sensor of ^{K27}Ub Chains

Because UCHL3 recognizes $^{K27}Ub_2$ with high specificity, we tested if UCHL3 could be a tool to detect K27 chains. We generated a catalytically inactive C95A UCHL3 with a C-terminal biotinylation tag (AviTag, Avidity LLC), biotinylated it, and used it for detection in western blot. Under these conditions, UCHL3 recognizes $^{K27}Ub_2$ over all other diubiquitin linkages (Figure 6F), similar to the existing K27-specific antibody (data not shown). Similar to other DUBs, mutating the catalytic cysteine to alanine (UCHL3 C95A) increases the affinity of UCHL3 for Ub (Morrow et al., 2018) or, in this case, K27-linked diubiquitin, making it useful as an affinity reagent. Taken together, these results make UCHL3 C95A AviTag an attractive and easily obtained tool to be used as an antibody or affimer to detect free $^{K27}Ub_2$ in western blot experiments.

Possible Roles for UCHL3 and $^{K27}Ub_2$ in Cell Signaling

In vitro, both free $^{K27}Ub_2$ and $^{K27}Ub_2$-conjugated substrates quickly and potently inhibit UCHL3. Conversely, UCHL3 can specifically detect free ^{K27}Ub chains over other linkages. The abundance of free K27-linked chains in cells is unknown, but ^{K27}Ub chains are hallmark signals of the innate immune response and are conjugated to virtually all of the sensors and effectors of the intracellular pathogen response pathway (van Huizen and Kikkert, 2020). In addition, K27-linked chains are involved in the regulation of the intracellular DNA damage response (Akutsu et al., 2016). It is possible that UCHL3 acts as a sensor for free or conjugated K27-linked chains in these pathways or, conversely, that K27-linked chains regulate UCHL3's activity. Corroborating this idea, UCHL3 is necessary for the orderly progression of both the immune response and the DNA damage pathway, although the mechanism is still unclear. However, because UCHL3 prefers to cleave smaller substrates (Figures 5A–5D and Navarro et al., 2014; Popp et al., 2009), we further speculate that $^{K27}Ub_{(n)}$-conjugated substrates that affect UCHL3 are likely to be small and/or disordered proteins. Recent work has shown the existence and importance of a large number of functional and abundant microproteins (10–100 residues) (Chen et al., 2020; Yin et al., 2019) that, if appropriately K27-ubiquitinated, could be viable targets for UCHL3. Our data showed an unusual kinetic response of UCHL3 to K27 chains. Further research will have to elucidate if and how this relationship affects host-pathogen interactions.

SIGNIFICANCE

K27-linked ubiquitin chains are a poorly understood type of ubiquitin modification, owing in part to the fact that they cannot be made enzymatically. Although not largely present in cells under normal conditions, they are upregulated during pathogenic infections and interact with virtually all players of the immune response pathway.

UCHL3 is one of only three deubiquitinating enzymes that show a strong preference for K27-linked diubiquitin. However, the relation between UCHL3 and K27 is not a simple preference for a substrate. Rather, using a series of specifically crafted ubiquitin tools, we show that $^{K27}Ub_2$ strongly inhibits UCHL3 activity, both when free and when conjugated to a substrate.

The mechanism of inhibition is unusual. $^{K27}Ub_2$ can form a thioester bond with UCHL3's catalytic cysteine and can adopt an inhibitory conformation that restrains UCHL3's crossover loop. At each cleavage cycle, there is a finite probability that $^{K27}Ub_2$ might adopt the inhibitory conformation, trapping UCHL3. Thus, the more K27-ubiquitinated substrates UCHL3 cleaves, the higher is the chance of it becoming inhibited. We dubbed this phenomenon a "kinetic trap."

The fact that the kinetic trap is specific for the K27 linkage and the observation that the levels of inhibition depend on the ratio of substrate to UCHL3 suggest that $^{K27}Ub_2$ and UCHL3 act as a signal-response pair. UCHL3 could be sensing K27-ubiquitinated substrate levels in the cell, or K27-ubiquitinated substrates could be dampeners of UCHL3 activity. Either way, since both UCHL3 and K27-linked ubiquitin chains play roles in the immune response, it seems possible that this mechanism is required for a proper response during innate immune reactions.

STAR★METHODS

Detailed methods are provided in the online version of this paper and include the following:

SUPPLEMENTAL INFORMATION

Supplemental Information can be found online at https://doi.org/10.1016/j.chembiol.2020.11.005.

ACKNOWLEDGMENTS

We thank M. Bower and MASSIF-1/ID30A staff for data collection; X. Guo for the Ub-His construct; the Vertegaal lab for the 3×SUMO2ΔN construct, the SUMO2 antibody, and the RNF4 protein; S. Dharadhar for PCNA reagents; P. Geurink for amino-propane-modified Rho; the NKI protein facility for BirA ligase production; L. Janssen for the pRP265-AviTAG vector; and R. Merkx for expression of the UCHL3 batch used for crystallization. Funding for this work was from the Oncode Institute (H.O.), Gravity Program CGC.nl (NWO) to T.K.S., VICI (NWO 724.013.002) to H.O., and VENI and VIDI (NWO) to G.J.v.d.H.v.N.

AUTHOR CONTRIBUTIONS

G.B.A.v.T. and A.G.M. conceived of and performed the experiments, analyzed the data, and wrote the manuscript with input from all authors. A.F. performed the stopped-flow experiments, assisted with data analysis, and performed the fitting of the kinetic model. G.J.v.d.H.v.N. performed the chemical synthesis of Ub substrates. H.O. and T.K.S. supervised and directed the project. All authors have given approval to the final version of the manuscript. G.B.A.v.T. and A.M. contributed equally to this work.

DECLARATION OF INTERESTS

The authors declare no competing interests.

Received: September 17, 2020
Revised: October 25, 2020
Accepted: November 4, 2020
Published: November 24, 2020

SUPPORTING CITATIONS

The following reference appears in the supplemental information: Edgar (2004).

REFERENCES

Akutsu, M., Dikic, I., and Bremm, A. (2016). Ubiquitin chain diversity at a glance. J Cell Sci. *129*, 875–880.

Bett, J.S., Ritorto, M.S., Ewan, R., Jaffray, E.G., Virdee, S., Chin, J.W., Knebel, A., Kurz, T., Trost, M., Tatham, M.H., et al. (2015). Ubiquitin C-terminal hydrolases cleave isopeptide- and peptide-linked ubiquitin from structured proteins but do not edit ubiquitin homopolymers. Biochem. J. *466*, 489–498.

Boudreaux, D.A., Chaney, J., Maiti, T.K., and Das, C. (2012). Contribution of active site glutamine to rate enhancement in ubiquitin C-terminal hydrolases. FEBS J. *279*, 1106–1118.

Bowler, M.W., Svensson, O., and Nurizzo, D. (2016). Fully automatic macromolecular crystallography: the impact of MASSIF-1 on the optimum acquisition and quality of data. Crystallogr. Rev. *22*, 233–249.

Bremm, A., Freund, S.M.V., and Komander, D. (2010). Lys11-linked ubiquitin chains adopt compact conformations and are preferentially hydrolyzed by the deubiquitinase Cezanne. Nat. Struct. Mol. Biol. *17*, 939–947.

Bustamante, C., Chemla, Y.R., Forde, N.R., and Izhaky, D. (2004). Mechanical processes in biochemistry. Annu. Rev. Biochem. *73*, 705–748.

Castaneda, C.A., Dixon, E.K., Walker, O., Chaturvedi, A., Nakasone, M.A., Curtis, J.E., Reed, M.R., Krueger, S., Cropp, T.A., and Fushman, D. (2016). Linkage via K27 bestows ubiquitin chains with unique properties among polyubiquitins. Structure *24*, 423–436.

Chen, J., Brunner, A.-D., Cogan, J.Z., Nuñez, J.K., Fields, A.P., Adamson, B., Itzhak, D.N., Li, J.Y., Mann, M., Leonetti, M.D., et al. (2020). Pervasive functional translation of noncanonical human open reading frames. Science *367*, 1140–1146.

Cook, W.J., Jeffrey, L.C., Carson, M., and Chenlal, Z. (1992). Structure of a diubiquitin conjugate and model for interaction with ubiquitin conjugating enzyme(E2). JBC *267*, 16467–16471.

Daiss, J.L., Nishitani, K., Schwarz, E.M., and Kates, S.L. (n.d.). Diagnostic Device And Method For Detection Of Staphylococcus Infection.

Dennissen, F.J.A., Kholod, N., Hermes, D.J.H.P., Kemmerling, N., Steinbusch, H.W.M., Dantuma, N.P., and van Leeuwen, F.W. (2011). Mutant ubiquitin (UBB+1) associated with neurodegenerative disorders is hydrolyzed by ubiquitin C-terminal hydrolase L3 (UCH-L3). FEBS Lett. *585*, 2568–2574.

Edgar, R.C. (2004). MUSCLE: multiple sequence alignment with high accuracy and high throughput. Nucleic Acids Res. *32*, 1792–1797.

Eifler, K., Cuijpers, S.A.G., Willemstein, E., Raaijmakers, J.A., El Atmioui, D., Ovaa, H., Medema, R.H., and Vertegaal, A.C.O. (2018). SUMO targets the APC/C to regulate transition from metaphase to anaphase. Nat. Commun. *9*, 1119.

El Oualid, F., Merkx, R., Ekkebus, R., Hameed, D.S., Smit, J.J., de Jong, A., Hilkmann, H., Sixma, T.K., and Ovaa, H. (2010). Chemical synthesis of ubiquitin, ubiquitin-based probes, and diubiquitin. Angew. Chem. Int. Ed. *49*, 10149–10153.

Emsley, P., Lohkamp, B., Scott, W.G., and Cowtan, K. (2010). Features and development of Coot. Acta Crystallogr. D Biol. Crystallogr. *66*, 486–501.

Evans, P.R., and Murshudov, G.N. (2013). How good are my data and what is the resolution? Acta Crystallogr. D Biol. Crystallogr. *69*, 1204–1214.

Flierman, D., van der Heden van Noort, G.J., Ekkebus, R., Geurink, P.P., Mevissen, T.E.T., Hospenthal, M.K., Komander, D., and Ovaa, H. (2016). Non-hydrolyzable diubiquitin probes reveal linkage-specific reactivity of deubiquitylating enzymes mediated by S2 pockets. Cell Chem. Biol. *23*, 472–482.

García-Nafría, J., Watson, J.F., and Greger, I.H. (2016). IVA cloning: a single-tube universal cloning system exploiting bacterial in Vivo Assembly. Sci. Rep. *6*, 27459.

Grou, C.P., Pinto, M.P., Mendes, A.V., Domingues, P., and Azevedo, J.E. (2015). The de novo synthesis of ubiquitin: identification of deubiquitinases acting on ubiquitin precursors. Sci. Rep. *5*, 12836.

Hemelaar, J., Borodovsky, A., Kessler, B.M., Reverter, D., Cook, J., Kolli, N., Gan-Erdene, T., Wilkinson, K.D., Gill, G., Lima, C.D., et al. (2004). Specific and covalent targeting of conjugating and deconjugating enzymes of ubiquitin-like proteins. Mol. Cell Biol. *24*, 84–95.

Hibbert, R.G., and Sixma, T.K. (2012). Intrinsic flexibility of ubiquitin on proliferating cell nuclear antigen (PCNA) in translesion synthesis. J. Biol. Chem. *287*, 39216–39223.

van Huizen, M., and Kikkert, M. (2020). The role of atypical ubiquitin chains in the regulation of the antiviral innate immune response. Front. Cell Dev. Biol. *7*, 392.

Johnson, K.A., Simpson, Z.B., and Blom, T. (2009a). Global Kinetic Explorer: a new computer program for dynamic simulation and fitting of kinetic data. Anal. Biochem. *387*, 20–29.

Johnson, K.A., Simpson, Z.B., and Blom, T. (2009b). FitSpace Explorer: an algorithm to evaluate multidimensional parameter space in fitting kinetic data. Anal. Biochem. *387*, 30–41.

Johnston, S.C., Larsen, C.N., Cook, W.J., Wilkinson, K.D., and Hill, C.P. (1997). Crystal structure of a deubiquitinating enzyme (human UCH-L3) at 1.8 Å resolution. EMBO J. *16*, 3787–3796.

Johnston, S.C., Riddle, S.M., Cohen, R.E., and Hill, C.P. (1999). Structural basis for the speci city of ubiquitin C-terminal hydrolases. EMBO J. *18*, 3877–3887.

Joosten, R.P., Long, F., Murshudov, G.N., and Perrakis, A. (2014). The *PDB_REDO* server for macromolecular structure model optimization. IUCrJ *1*, 213–220.

Kabsch, W. (2010). Integration, scaling, space-group assignment and post-refinement. Acta Crystallogr. Section D Biol. Crystallogr. *66*, 133–144.

Kim, J.Y., Lee, J.-M., and Cho, J.-Y. (2011). Ubiquitin C-terminal hydrolase-L3 regulates Smad1 ubiquitination and osteoblast differentiation. FEBS Lett. *585*, 1121–1126.

Kim, R.Q., Geurink, P.P., Mulder, M.P.C., Fish, A., Ekkebus, R., El Oualid, F., van Dijk, W.J., van Dalen, D., Ovaa, H., van Ingen, H., et al. (2019). Kinetic analysis of multistep USP7 mechanism shows critical role for target protein in activity. Nat. Commun. *10*, 231.

Komander, D., and Rape, M. (2012). The ubiquitin code. Annu. Rev. Biochem. *81*, 203–229.

Krissinel, E., and Henrick, K. (2004). Secondary-structure matching (SSM), a new tool for fast protein structure alignment in three dimensions. Acta Crystallogr. D Biol. Crystallogr. *60*, 2256–2268.

Kristariyanto, Y.A., Abdul Rehman, S.A., Campbell, D.G., Morrice, N.A., Johnson, C., Toth, R., and Kulathu, Y. (2015). K29-Selective ubiquitin binding domain reveals structural basis of specificity and heterotypic nature of K29 polyubiquitin. Mol. Cell *58*, 83–94.

Kurihara, L.J. (2001). Loss of Uch-L1 and Uch-L3 leads to neurodegeneration, posterior paralysis and dysphagia. Hum. Mol. Genet. *10*, 1963–1970.

Lai, M.-Y., Zhang, D., LaRonde-LeBlanc, N., and Fushman, D. (2012). Structural and biochemical studies of the open state of Lys48-linked diubiquitin. Biochim. Biophys. Acta *1823*, 2046–2056.

Larsen, C.N., Krantz, B.A., and Wilkinson, K.D. (1998). Substrate specificity of deubiquitinating enzymes: ubiquitin C-terminal hydrolases †. Biochemistry *37*, 3358–3368.

Liao, C., Beveridge, R., Hudson, J.J.R., Parker, J.D., Chiang, S.-C., Ray, S., Ashour, M.E., Sudbery, I., Dickman, M.J., and El-Khamisy, S.F. (2018). UCHL3 regulates topoisomerase-induced chromosomal break repair by controlling TDP1 proteostasis. Cell Rep. *23*, 3352–3365.

Luna-Vargas, M.P.A., Christodoulou, E., Alfieri, A., van Dijk, W.J., Stadnik, M., Hibbert, R.G., Sahtoe, D.D., Clerici, M., Marco, V.D., Littler, D., et al. (2011). Enabling high-throughput ligation-independent cloning and protein expression for the family of ubiquitin specific proteases. J. Struct. Biol. *175*, 113–119.

Luo, K., Li, L., Li, Y., Wu, C., Yin, Y., Chen, Y., Deng, M., Nowsheen, S., Yuan, J., and Lou, Z. (2016). A phosphorylation-deubiquitination cascade regulates the BRCA2-RAD51 axis in homologous recombination. Genes Dev. *30*, 2581–2595.

Matsumoto, M.L., Wickliffe, K.E., Dong, K.C., Yu, C., Bosanac, I., Bustos, D., Phu, L., Kirkpatrick, D.S., Hymowitz, S.G., Rape, M., et al. (2010). K11-Linked polyubiquitination in cell cycle control revealed by a K11 linkage-specific antibody. Mol. Cell *39*, 477–484.

McCoy, A.J., Grosse-Kunstleve, R.W., Adams, P.D., Winn, M.D., Storoni, L.C., and Read, R.J. (2007). *Phaser* crystallographic software. J. Appl. Crystallogr. *40*, 658–674.

McNicholas, S., Potterton, E., Wilson, K.S., and Noble, M.E.M. (2011). Presenting your structures: the CCP4mg molecular-graphics software. Acta Crystallogr. Section D Biol. Crystallogr. *67*, 386–394.

Mevissen, T.E.T., and Komander, D. (2017). Mechanisms of deubiquitinase specificity and regulation. Annu. Rev. Biochem. *86*, 159–192.

Michel, M.A., Elliott, P.R., Swatek, K.N., Simicek, M., Pruneda, J.N., Wagstaff, J.L., Freund, S.M.V., and Komander, D. (2015). Assembly and specific recognition of K29- and K33-linked polyubiquitin. Mol. Cell *58*, 95–109.

Misaghi, S., Galardy, P.J., Meester, W.J.N., Ovaa, H., Ploegh, H.L., and Gaudet, R. (2005). Structure of the ubiquitin hydrolase UCH-L3 complexed with a suicide substrate. J. Biol. Chem. *280*, 1512–1520.

Morrow, M.E., Morgan, M.T., Clerici, M., Growkova, K., Yan, M., Komander, D., Sixma, T.K., Simicek, M., and Wolberger, C. (2018). Active site alanine mutations convert deubiquitinases into high-affinity ubiquitin-binding proteins. EMBO Rep. *19*, e45680.

Mtango, N.R., Sutovsky, M., Vandevoort, C.A., Latham, K.E., and Sutovsky, P. (2012). Essential role of ubiquitin C-terminal hydrolases UCHL1 and UCHL3 in mammalian oocyte maturation. J. Cell Physiol. *227*, 2022–2029.

Murshudov, G.N., Skubák, P., Lebedev, A.A., Pannu, N.S., Steiner, R.A., Nicholls, R.A., Winn, M.D., Long, F., and Vagin, A.A. (2011). *REFMAC* 5 for the refinement of macromolecular crystal structures. Acta Crystallogr. Section D Biol. Crystallogr. *67*, 355–367.

Navarro, M.F., Carmody, L., Romo-Fewell, O., Lokensgard, M.E., and Love, J.J. (2014). Characterizing substrate selectivity of ubiquitin C-terminal hydrolase-L3 using engineered alpha-linked ubiquitin substrates. Biochemistry *53*, 8031–8042.

Nishi, R., Wijnhoven, P.W.G., Kimura, Y., Matsui, M., Konietzny, R., Wu, Q., Nakamura, K., Blundell, T.L., and Kessler, B.M. (2018). The deubiquitylating enzyme UCHL3 regulates Ku80 retention at sites of DNA damage. Scientific Rep. *8*, 17891.

Pan, M., Zheng, Q., Ding, S., Zhang, L., Qu, Q., Wang, T., Hong, D., Ren, Y., Liang, L., Chen, C., et al. (2019). Chemical protein synthesis enabled mechanistic studies on the molecular recognition of K27-linked ubiquitin chains. Angew. Chem. Int. Ed. *58*, 2627–2631.

Pickart, C.M., and Rose, I.A. (1986). Mechanism of ubiquitin carboxyl-terminal hydrolase. Borohydride and hydroxylamine inactivate in the presence of ubiquitin. J. Biol. Chem. *261*, 10210–10217.

Popp, M.W., Artavanis-Tsakonas, K., and Ploegh, H.L. (2009). Substrate filtering by the active site crossover loop in UCHL3 revealed by sortagging and gain-of-function mutations. J. Biol. Chem. *284*, 3593–3602.

Rohaim, A., Kawasaki, M., Kato, R., Dikic, I., and Wakatsuki, S. (2012). Structure of a compact conformation of linear diubiquitin. Acta Crystallogr. Section D Biol. Crystallogr. *68*, 102–108.

Sato, Y., Yoshikawa, A., Mimura, H., Yamashita, M., Yamagata, A., and Fukai, S. (2009). Structural basis for specific recognition of Lys 63-linked polyubiquitin chains by tandem UIMs of RAP80. EMBO J. *28*, 2461–2468.

Scholz, J., Besir, H., Strasser, C., and Suppmann, S. (2013). A new method to customize protein expression vectors for fast, efficient and background free parallel cloning. BMC Biotechnol. *13*, 12.

Semenova, E., Wang, X., Jablonski, M.M., Levorse, J., and Tilghman, S.M. (2003). An engineered 800 kilobase deletion of Uchl3 and Lmo7 on mouse chromosome 14 causes defects in viability, postnatal growth and degeneration of muscle and retina. Hum. Mol. Genet. *12*, 1301–1312.

Vertegaal, A.C.O., Ogg, S.C., Jaffray, E., Rodriguez, M.S., Hay, R.T., Andersen, J.S., Mann, M., and Lamond, A.I. (2004). A proteomic study of SUMO-2 target proteins. J. Biol. Chem. *279*, 33791–33798.

Vijay-kumar, S., Bugg, C.E., and Cook, W.J. (1987). Structure of ubiquitin refined at 1.8 Å resolution. J. Mol. Biol. *194*, 531–544.

Virdee, S., Ye, Y., Nguyen, D.P., Komander, D., and Chin, J.W. (2010). Engineered diubiquitin synthesis reveals Lys29-isopeptide specificity of an OTU deubiquitinase. Nat. Chem. Biol. *6*, 750–757.

Wada, H., Kito, K., Caskey, L.S., Yeh, E.T., and Kamitani, T. (1998). Cleavage of the C-terminus of NEDD8 by UCH-L3. Biochem. Biophys. Res. Commun. *251*, 688–692.

Waterhouse, A.M., Procter, J.B., Martin, D.M.A., Clamp, M., and Barton, G.J. (2009). Jalview Version 2–a multiple sequence alignment editor and analysis workbench. Bioinformatics *25*, 1189–1191.

Winn, M.D., Ballard, C.C., Cowtan, K.D., Dodson, E.J., Emsley, P., Evans, P.R., Keegan, R.M., Krissinel, E.B., Leslie, A.G.W., McCoy, A., et al. (2011). Overview of the CCP4 suite and current developments. Acta Crystallogr. Section D Biol. Crystallogr. *67*, 235–242.

Yi, Y.-J., Manandhar, G., Sutovsky, M., Li, R., Jonakova, V., Oko, R., Park, C.-S., Prather, R.S., and Sutovsky, P. (2007). Ubiquitin C-terminal hydrolase-activity is involved in sperm acrosomal function and anti-polyspermy defense during porcine fertilization. Biol. Reprod. *77*, 780–793.

Yin, X., Jing, Y., and Xu, H. (2019). Mining for missed sORF-encoded peptides. Expert Rev. Proteomics *16*, 257–266.

Zhang, X., Smits, A.H., van Tilburg, G.B.A., Jansen, P.W.T.C., Makowski, M.M., Ovaa, H., and Vermeulen, M. (2017). An interaction landscape of ubiquitin signaling. Mol. Cell *65*, 941–955.e8.

Zhao, P., Guo, T., Qian, L., Wang, X., Yuan, Y., Cheng, Q., Zuo, Y., Liu, J., Miao, Y., Feng, Q., et al. (2017). Ubiquitin C-terminal hydrolase-L3 promotes interferon antiviral activity by stabilizing type I-interferon receptor. Antivir. Res *144*, 120–129.

Zhou, Z.-R., Zhang, Y.-H., Liu, S., Song, A.-X., and Hu, H.-Y. (2012). Length of the active-site crossover loop defines the substrate specificity of ubiquitin C-terminal hydrolases for ubiquitin chains. Biochem. J. *441*, 143–149.

STAR★METHODS

KEY RESOURCES TABLE

REAGENT or RESOURCE	SOURCE	IDENTIFIER
Antibodies		
Anti SUMO2 (rabbit polyclonal)	Life Technologies	Cat#519100
Anti Ubiquitin (mouse)	Santa Cruz	Cat#P4D1
neutravidin DyLight800	Thermo Fisher Scientific	Cat#22853
donkey-α-rabbit IRDye®680	LI-COR	Cat# 926-68073; RRID: AB_10954442
goat-α-mouse IRDye®800	LI-COR	Cat#926-32210; RRID: AB_621842
Goat Anti-Mouse IgG (H + L)-HRP Conjugate	Bio Rad	Cat#170-6516; RRID: AB_11125547
Goat Anti-Rabbit IgG (H + L)-HRP Conjugate	Bio Rad	Cat#1706515; RRID: AB_2617112
Bacterial and Virus Strains		
Escherichia coli BL21(DE3) T1 phage resistant	New England Biosciences	Cat#C2527H
Chemicals, Peptides, and Recombinant Proteins		
$^{K27}Ub_2$	El Oualid et al., 2010	N/A
$^{K63}Ub_2$	El Oualid et al., 2010	N/A
Ub-Rho	El Oualid et al., 2010	N/A
$^{K27}Ub_2$-Rho	Flierman et al., 2016	N/A
$^{K63}Ub_2$-Rho	Flierman et al., 2016	N/A
Ub-L40-Rho	This paper	N/A
$^{K27}Ub_2$-L40-Rho	This paper	N/A
Ub-His	This paper	N/A
Ub-SUMO2	This paper	N/A
3xSUMO2ΔN11	Eifler et al., 2018	N/A
UCHL3	This paper	N/A
UCHL3 E158R	This paper	N/A
UCHL3 E158A	This paper	N/A
UCHL3 C95S	This paper	N/A
UCHL3 C95A	This paper	N/A
His-SUMO-UCHL3	This paper	N/A
His-SUMO-UCHL3 C95A	This paper	N/A
His-SUMO-UCHL3 C95S	This paper	N/A
Biotinylated UCHL3 C95A	This paper	N/A
Ub-PCNA	Hibbert and Sixma, 2012	N/A
Ub(n)-3xSUMO2ΔN	This paper	N/A
Critical Commercial Assays		
SA chip Biacore	Cytiva Life Sciences	Cat#29104992
Deposited Data		
UCHL3	Johnston et al., 1997	PDB: 1UCH
UCHL3-UbVME	Misaghi et al.	PDB: 1XD3
UCHL3-Lym27Ub_2	Pan et al., 2019	PDB: 6ISU
K6-linked diubiquitin	Virdee et al., 2010	PDB: 2XK5
K11-linked diubiquitin	Bremm et al., 2010	PDB: 2XEW
K11-linked di-ubiquitin	Matsumoto et al., 2010	PDB: 3NOB
TRABID NZF1- K29 linked di-Ubiquitin	Kristariyanto et al., 2015	PDB: 4S1Z
K29 linked di-Ubiquitin	Kristariyanto et al., 2015	PDB: 4S22

(*Continued on next page*)

Continued

REAGENT or RESOURCE	SOURCE	IDENTIFIER
K33-linked diubiquitin	Michel et al., 2015	PDB: 5AF4
TRABID NZF1-K33-linked diubiquitin	Michel et al., 2015	PDB: 5AF6
K48-linked di-ubiquitin	Cook et al., 1992	PDB: 1AAR
K48-linked di-ubiquitin	Lai et al., 2012	PDB: 3NS8
RAP80 UIM-K63-linked di-ubiquitin	Sato et al., 2009	PDB: 3A1Q
Linear diubiquitin	Rohaim et al., 2012	PDB: 3AXC
K27-linked di-ubiquitin	Castaneda et al., 2016	PDB: 5UJN
UCHL3-$^{K27}Ub_2$ structure factors and model	This paper	PDB: 6QML
Recombinant DNA		
pET3a Ubiquitin-His	This paper	N/A
pET-NKI-1.1-His-3C-UbSUMO2	This paper	N/A
pHis-TEV30a-3xSUMO2ΔN11	Eifler et al., 2018	N/A
pRP265-GST-UCHL3	This paper	N/A
pRP265- GST-UCHL3 C95A	This paper	N/A
pRP265- GST-UCHL3 E158A	This paper	N/A
pRP265- GST-UCHL3 E158R	This paper	N/A
pRP265- GST-UCHL3-AviTag	This paper	N/A
pETNKI-1.10-HisSUMO2-UCHL3	This paper	N/A
pETNKI-1.10-HisSUMO2-UCHL3 C95A	This paper	N/A
pETNKI-1.10-HisSUMO2-UCHL3 C95S	This paper	N/A
Software and Algorithms		
CCD^2 – Crystallization Construct Designer	Murachelli et al., unpublished	https://ccd.rhpc.nki.nl
GraphPad Prism 7.0	GraphPad Software	RRID:SCR_002798
Kintek Explorer	KinTek	https://kintekcorp.com/software
CCP4MG	McNicholas et al., 2011	RRID: SCR_019041
CCP4	Winn et al., 2011	RRID:SCR_007255
Phaser	McCoy et al., 2007	RRID:SCR_014219
PDB_REDO	Joosten et el., 2014	RRID:SCR_018936
Coot	Emsley et al., 2010	RRID:SCR_014222
Jalview	Waterhouse et al., 2009	RRID:SCR_006459

RESOURCE AVAILABILITY

Lead Contact

Further information and requests for resources and reagents should be directed to and will be fulfilled by the Lead Contact, Prof. Titia Sixma (t.sixma@nki.nl).

Materials Availability

Plasmids

The pETNKI vectors (Luna-Vargas et al., 2011) are available through Addgene; all constructs generated are available on request or through Addgene.

Synthetic Proteins

Protocols to generate synthetic diUb-reagents and recombinant proteins are included in the Materials & Methods section. Native isopeptide linked diubiquitin reagents are available via Boston Biochem. Other synthetic and semi-synthetic substrates are custom made and questions regarding assistance with synthesis can be addressed to gvanderheden@lumc.nl.

Data and Code Availability

The accession number for structure factors and model coordinates for the UCHL3:$^{K27}Ub_2$ crystal structure reported in this paper is PDB: 6QML

Further details and raw data for the Kintek model are available on request.

EXPERIMENTAL MODEL AND SUBJECT DETAILS

Bacterial Strains

All recombinant proteins were expressed in *Escherichia coli* strain BL21 (DE3), T1 Phage resistant (New England Biosciences Cat#C2527H). Details of culture and expression conditions for each recombinant construct are specified in Method Details.

METHOD DETAILS

Capture of the Thioester UCHL3~$^{K27}Ub_2$ Bond by $NaBH_4$

Mono Ub (10 μg/mL) and UCHL3 (10 μg/mL) or $^{K27}Ub_2$ (20 μg/mL) and UCHL3 (10 ug/mL) were incubated for 90 minutes at 37 °C in 200 μL buffer (50 mM Tris-HCl pH 7.6, 5 mM DTT, 1 mM EDTA). Subsequently, 1 mM of $NaBH_4$ was added 6 times in total with an interval of 5 minutes between each new addition (total incubation time 30 minutes, final concentration 6 mM $NaBH_4$). 1 M formic acid was added for 5 minutes before final measurement on a Waters Xevo-G2 XS Q-TOF mass spectrometer equipped with an electrospray ion source in positive mode (source voltage 3.0 kV, desolvation gas flow 900L/h, temperature 250°C) with resolution R = 22000 (mass range m/z = 50-2000) and 200 pg/μl Leu-Enk (m/z = 556.2771) as "lock mass"). Samples were run according to the following protocol: 0 - 4 minutes in 2% B (1% H_2O and 0.1% formic acid in CH_3CN), a gradient from 2% to 100% B over 7.5 minutes (4 – 11.5 minutes), 0.5 minute at 100% B (11.5 – 12 minutes) and a reduction to 2% B and 98% A (H_2O with 0.1% formic acid) in 2 minutes (12.10 – 14.00 minutes). Reaction products were separated on an Acquity UPLC Protein BEH C4 300 Angstrom column (1.7 μm, 2.1 mm x 50 mm) at 60 °C using a flow rate of 0.5 mL/min. Data processing was performed using Waters MassLynx Mass Spectrometry Software 4.1.

Synthesis of Ubiquitin and Diubiquitin Species

Solid phase peptide synthesis (SPPS) was performed on a Syro II MultiSyntech Automated Peptide synthesizer using standard 9-fluorenylmethoxycarbonyl (Fmoc) based solid phase peptide chemistry at 25 μmol scale, using fourfold excess of amino acids relative to pre-loaded Fmoc amino acid trityl resin (0.2 mmol/g, Rapp Polymere GmbH). All synthetic products were assayed for purity by high resolution mass spectrometry on a Waters Acquity H-class UPLC with XEVO-G2 XS Q-TOF mass spectrometer and by SDS PAGE analysis.

Ub-Rho

Ub-Rho was prepared using the methodology described in (El Oualid et al., 2010). Briefly, Ub^{1-75} was synthesised using SPPS and liberated from the resin using 20% v/v HFIP in DCM while leaving all protective groups in place. After concentration of the crude material, subsequent activation of the C-terminal carboxylate of Gly75 using HBTU/HOBt allowed coupling of bis-glycine-rhodamine-110. Treatment with 95% TFA removed all protective groups. Precipitation from Et_2O/Pentane 1:1, v/v followed by RP-HPLC purification and lyophilization of the appropriate fractions yielded the Ub-Rho product.

Biotin-Ub and Non-hydrolysable Biotin-$^{K27/K63}Ub_2$

N-terminally biotinylated mono Ub was prepared as described in (Zhang et al., 2017). Briefly, Ub^{1-76} was synthesized using automated SPPS and afterwards a PEG spacer (8-(amino)-3,6-dioxaoctanoic acid) and biotin were coupled on the N-terminus. Biotinylated $^{K63}Ub_2$ and $^{K63}Ub_2$ were prepared using copper(I)-catalyzed Azide-Alkyne cycloaddition (CuAAC). In brief, distal biotinylated Ub-propargylamide was prepared by coupling propargylamine to partially protected Ub^{1-75} using 5 eq. PyBOP, 5 eq. triethylamine and 10 eq. propargylamine (PA). The proximal ubiquitin moieties were constructed using SPPS where azide containing lysine analog (Fmoc-L-azidoornithine, Chiralix CX25404) was incorporated at the respective lysine position. Treatment with 95% TFA removed all protective groups and precipitation from Et_2O/Pentane 1:1, v/v followed by HPLC purification yielded the pure distal and proximal Ub mutants. CuAAC reactions were performed under argon and in 8M urea/100 mM phosphate pH 7 using 1.25 mM $CuSO_4$, 7.5 mM sodium ascorbate and 1.25 mM TBTA (1,1',1''-Tris(1H-1,2,3-triazol-4-yl-1-acetic acid ethyl ester) trimethylamine, Carbosynth). DiUb products were purified by RP-HPLC (detailed below) and size exclusion (S75 16/60 PG, GE healthcare) in 20 mM Tris-HCl pH 7.6, 150 mM NaCl.

Ub-AMC, $^{K27}Ub_2$-AMC, $^{K63}Ub_2$-AMC

Ub-AMC was prepared as described in (El Oualid et al., 2010). Briefly, Ub^{1-75} was synthesised using SPPS and liberated from the resin using 20% v/v HFIP in DCM while leaving all protective groups in place. After concentration of the crude material, subsequent activation of the C-terminal carboxylate of Gly75 using HBTU/HOBt allowed coupling of glycine-AMC. Treatment with 95% TFA removed all protective groups. Precipitation from Et_2O/Pentane 1:1, v/v followed by RP-HPLC purification and lyophilization of the appropriate fractions yielded the Ub-AMC product.$^{K63}Ub_2$-AMC and $^{K27}Ub_2$-AMC were prepared as described in (Flierman et al., 2016). Briefly, Ub-propargylamide was coupled to Ub-AMC, containing azido-ornithine at the indicated lysine position, using CuAAC conditions described above. Products were purified by RP-HPLC (detailed below) and size exclusion (S75 16/60 PG, GE healthcare) in 20 mM Tris-HCl pH 7.6, 150 mM NaCl.

$^{K27}Ub_2$ ($^{K27}Ub_2$Met1NLE)

$^{K27}Ub_2$ was prepared similarly to the protocol described in (El Oualid et al., 2010). We substituted methione for norleucine on position 1 of the proximal ubiquitin to avoid oxidation during synthesis; the norleucine residue has no contact with UCHL3, and the construct behaves like wild type Ub_2. Met1 on the distal ubiquitin is not substituted. In brief, tert-butylthio (StBu)-protected Met1NLE Lys27 γ-thiolysine Ub (16.5 mg) was dissolved in 100 μL DMSO and added to 350 μL of 8 M Guanidium-HCl (Gdn.HCl)/100 mM phosphate

buffer at pH 7.6 supplemented with 50 μL 1 M tris(2-carboxy-ethyl)phosphine (TCEP) and reacted at 37 °C. After LC-MS analysis revealed complete deprotection of the thiolysine, 1 equivalent of Ub-thioester dissolved in 100 μL DMSO and 400 μL 8 M Gdn.HCl/100 mM phosphate buffer at pH 7.6 and 100 μL 1M 4-Mercaptophenylacetic acid (MPAA) were added. The pH was adjusted to 7.6 and the mixture reacted for 16 hours at 37 °C. RP-HPLC purification was followed by lyophilization of the appropriate fractions. The lyophylized $^{K27}Ub_2$ (~30 mg) was desulfurized by dissolving in 200 μL dimethyl sulfoxide (DMSO) and subsequent dilution into 6 mL 8 M Gdn.HCl/100 mM phosphate buffer at pH 7.6 and 1 mL 1M TCEP. 2,2'-Azobis[2-(2-imidazolin-2-yl)propane] Dihydrochloride (VA044) (25 mg/mL) and reduced glutathione (GSH, 25 mg/mL) were added, pH was adjusted to 7.0 and the reaction was agitated for 16 hours at 37 °C. RP-HPLC purification was followed by lyophilization of the appropriate fractions. The lyophilized $^{K27}Ub_2$ was dissolved in 200 μL DMSO and diluted into 1800 μL 20 mM TRIS, 150 mM NaCl at pH 7.6, purified on a S75 16/600 Sephadex size exclusion column (GE healthcare) and concentrated to 7.2 mg/mL by spin filtration. The aliquots were snap frozen and stored at -80 °C until further use. Diubiquitins of other linkages (including $^{K63}Ub_2$) were prepared similarly using tert-butyl thiol (StBu)-protected Met1NLE, Lys(X) γ-thiolysine Ub as the proximal ubiquitin, where X is the lysine on the proximal ubiquitin to be linked.

Ub-L40-Rho

Ub-L40 (ubiquitin fused to the decapeptide IIEPSLRQLA with rhodamine on the C-terminus) was prepared on trityl resin using automated synthesis and its N-terminus was protected with a BOC group by treatment with Boc_2O (5 equivalents) and DiPEA (15 equivalents) in DCM for 2 hours. Subsequently the resin was washed with DCM and the peptide liberated from the resin while leaving all protective groups in place by reacting the resin 2 times for 20 minutes with 20 % v/v HFIP/DCM. The collected filtrates were concentrated, co-evaporated with dichloroethane three times and put under high vacuum for 30 minutes before further use. Amino-propane modified rhodamine (3 equivalents, synthesis described below) was coupled to the C-terminus of the peptide using HBTU (3 equivalents), HOBt (3 equivalents) and DiPEA (9 equivalents) in DCM for 16 hours at room temperature. Treatment of the resin using 95% TFA liberated the peptide from the resin and removed all protective groups. Precipitation from Et_2O/Pentane 1:1, v/v followed by RP-HPLC purification and size exclusion (S75 16/60 PG, GE healthcare) in 20 mM Tris-HCl pH 7.6, 150 mM NaCl yielded the Ub-L40-Rho product.

Synthesis of Rho(Boc)$_2$-NH(CH$_2$)$_3$N$_3$

N,N'-diBoc-5-carboxyrhodamine (206 mg, 0.36 mmol) was dissolved in DCM (10 mL). DiPEA (4.5 eq., 1.62 mmol, 285 μL), HCTU (1.5 eq., 0.54 mmol, 223 mg) and 3-azido-1-propanamine (1.5 eq., 0.54 mmol, 53 μL) were added and the mixture was stirred until TLC analysis indicated a complete conversion after 30 min. The mixture was diluted with 20 mL DCM and extracted with 0.1 M HCl_{aq} (2x), saturated aqueous $NaHCO_3$ (2x) and brine and dried over $MgSO_4$. Celite was added and the mixture was concentrated to dryness under reduced pressure. The compound bound to Celite was loaded onto a 24g silica column and purified on a Büchi automated column chromatography system using a 10 → 100% v/v ethyl acetate/*n*-heptane gradient. The product was obtained as a pale yellow solid (yield: 160 mg, 0.24 mmol, 68%).

Synthesis of Rho(Boc)$_2$-NH(CH$_2$)$_3$NH$_2$

Rho(Boc)$_2$-NH(CH$_2$)$_3$N$_3$ (160 mg, 0.24 mmol) was dissolved in THF (5 mL) and to this were added H_2O (100 μL) and trimethylphosphine (6 eq., 1.44 mmol, 1.44 mL of a 1M solution in THF) and the reaction was stirred for 15 hours after which TLC analysis indicated a complete consumption of starting material. The mixture was concentrated to dryness under reduced pressure and co-evaporated with toluene three times. The residue was dissolved in 20 mL ethyl acetate and extracted with saturated aqueous $NaHCO_3$ (2x) and brine, dried over $MgSO_4$ and concentrated. The product was obtained as a pale yellow solid (yield: 150 mg, 0.23 mmol, 98%).

^{K27}Ub$_2$-L40-Rho

$^{K27}Ub_2$-L40-Rho was prepared analogously to Ub-L40-Rho, except StBu-protected K27-γ-thiolysine-Ub-L40 was used as starting material to obtain K27-γ-thiolysine-Ub-L40-Rho. Native chemical ligation and desulfurization as described for $^{K27}Ub_2$ was then performed to provide the target $^{K27}Ub_2$- L40-Rho.

Reverse Phase, High Performance Liquid Chromatography (RP-HPLC) Purifications

RP-HPLC purification were carried out on a Waters preparative RP-HPLC system equipped with a Waters C18-Xbridge 5 μm OBD (10 x 150 mm) column at a flowrate of 37.5 mL/min. using 3 mobile phases: A: MQ, B: CH_3CN and C: 1% TFA in MQ. Prep-HPLC program: Gradient: 0 – 5 min: 5% B, 5%C; 5 – 7 min: 5 -> 20% B, 5% C; 7 – 18 min: 20 -> 45% B, 5% C, on a Waters C18-Xbridge 5 μm OBD (30 x 150 mm) column at a flow rate of 37.5 mL/min. Pure fractions were pooled and lyophilized.

Recombinant Protein Cloning, Expression and Purification

Escherichia coli strain BL21 (DE3), T1 Phage resistant, was transformed according to standard protocol. After transformation, a single colony was amplified overnight in Luria Bertani broth (LB) at 37°C and used as inoculum for large scale expression. Protein expression was carried out using 500 ml of medium in 3.5-liter, baffled Fernbach flasks, with 50 μl Antifoam 204 (Sigma-Aldrich) added to avoid foam. Flasks were shaken at 120 rpm during growth. Induction details vary for each construct and are indicated under each subheading. Pellets were harvested by centrifugation and used fresh, or frozen in liquid nitrogen and stored at -20°C.

Ub-His

Human ubiquitin was subcloned in a pET3a vector derivative encoding for a C-terminal His tag, resulting in the final protein sequence (Ubiquitin1-76)-DHHHHHH. Protein expression was carried out in Terrific Broth (TB). Cells were grown at 37°C to an optical density of 1.5, then induced with 0.5 mM isopropyl-thiogalactoside (IPTG) for 3 hours. Pellets were harvested and resuspended in lysis buffer (300 mM NaCl, 20 mM 4-(2-hydroxyethyl)-1-piperazineethanesulfonic acid (HEPES), pH 8.0) and lysed with two passes through an Avestin emulsiflex C5 (Avestin) at 200 kPa of pressure. The lysate was clarified by centrifugation (75000 g, 45 minutes, Avanti JXN26 centrifuge and JA25.50 rotor, Beckman Coulter) and applied with a peristaltic pump (flow 2 ml/min) to 10 ml of chelating sepharose resin

(GE healthcare) preloaded with Ni2+, pre-equilibrated in lysis buffer and packed in an HK-16/30 column holder (GE healthcare). The column was then washed with 1M NaCl, 20 mM HEPES pH 8.2, transferred to an AKTA or DuoLogic Bioflow liquid chromatography system (GE healthcare / Biorad, respectively), washed further with 300 mM NaCl, 50 mM imidazole pH 8.0, 20 mM HEPES. The protein was eluted using gel filtration buffer (100 mM NaCl, 20 mM HEPES pH 8.2) supplemented with 250 mM imidazole pH 8.0, dialysed overnight against gel filtration buffer + 5 mM dithiothreitol (DTT), concentrated by ultrafiltration (Amicon ultra, 3000 MWCO) and further purified by size exclusion chromatography (Superdex 75 16/60, GE healthcare or ENrich SEC 70 10/300, Biorad). The resulting pure protein was concentrated, aliquoted, flash frozen and stored at -80°C. All steps after lysis were carried out at 4°C or on ice.

Ub-SUMO2

The Ub-SUMO2 construct encodes a single copy of ubiquitin (Uniprot ID: P0CG48, residues 1-76) N-terminally fused to SUMO2 (Uniprot ID: P61956) and was synthesized as a gene block (IDT DNA) and subcloned in the pET-NKI-1.1-His3C-Kan vector (encoding for a 3C protease-cleavable hexahistidine tag, addgene #108703, Luna-Vargas et al., 2011) using ligation independent cloning (Scholz et al., 2013). Expression and purification followed the same protocol as Ub-His, but the hexahistidine tag was removed by 3C protease cleavage (NKI protein facility) during overnight dialysis prior to gel filtration.

3xSUMO2ΔN11

A pHis-TEV30a encoding a decahistidine-tagged 3xSUMO2ΔN11 construct was a kind gift from Prof. A. Vertegaal. For purification, we used a protocol adapted from (Eifler et al., 2018). Briefly, His10-tagged 3xSUMO2 was expressed in BL21 cells using 500 mL LB media in 2.5 liter baffled shaking flasks. Protein expression was induced at OD600 = 0.6 with 0.5 mM IPTG and overnight incubation at 18 °C. Cells were lysed through sonification on ice in 20 mM Tris-HCl pH 7.6, 150 mM NaCl, 25 mM $MgCl_2$, 5 mM dithiothreitol (DTT), 15 μg/mL DNAse I (Roche), 10 mM imidazole and 1x Complete protease inhibitor without EDTA (Roche).The protein was captured by affinity purification using 2 mL Ni-NTA beads (Qiagen) in a Poly-Prep Chromatograohy column (BioRad) and eluted two times at 4 °C in 5 mL 500 mM imidazole, 20 mM Tris-HCl pH 7.6, 150 mM NaCl, 5 mM DTT. After elution, the N-terminal His10 tag was removed by TEV protease and a final size exclusion step (S75 16/60 PG, GE healthcare) was performed in 20 mM Tris pH 7.6, 150 mM NaCl, 5 mM DTT.

Wild type UCHL3, UCHL3 E158A, UCHL3 E158R

Human UCHL3 (Uniprot ID: P15374) was cloned in pRP265, a pGEX-2T derivative, using IVA cloning (García-Nafría et al., 2016) and expressed in E. coli BL21(DE3) as N-terminal Glutathione-S-transferase (GST) fusion. Cells were grown in baffled shaking flasks containing LB medium and grown to an absorbance of 0.8 at 600 nm before induction with 0.5 mM IPTG. Cells were pelleted by centrifugation and resuspended in 40 mL lysis buffer (50 mM Tris pH 7.5, 10 mM DTT, 50 μM PMSF (Sigma), 1 mM EDTA, 10 mM $MgCl_2$). Lysozyme was added to 10.000 U/mL and incubated for 30 min. at 4 °C, after which the suspension was sonicated. The lysate was incubated with 2 mL glutathione sepharose 4B (GE healthcare) O/N at 4°, while rolling in a 50 mL Falcon tube. The next day, beads were washed 5 times with 50 mL buffer A (50 mM Tris pH 7.5, 0.5 mM EDTA, 5 mM DTT) and UCHL3 was cleaved from the beads with thrombin protease (3 hours, RT), leaving a Gly-Ser remnant at the N-terminus. After a reverse affinity purification step to remove residual GST traces, the protein was gel filtered in buffer A (Superdex75 16/60 PG, GE healthcare). Purified protein fractions were analyzed by SDS-PAGE and LC-MS (LCT^{TM} Orthogonal Acceleration Time of Flight Mass spectrometer, Micromass). The appropriate fractions were concentrated, aliquoted, flash frozen and stored at -80 °C.

His-SUMO-UCHL3

Human UCHL3 was cloned in pETNKI-1.10-HisSUMO-Kan vector (Luna-Vargas et al., 2011), encoding for a N-terminal hexahistidine SUMO2 tag. Cells were grown in shaking, baffled Fernbach flasks (3L, Schott) using 500 ml of terrific broth (TB) medium per flask until optical density of 1.5 and protein expression was induced by addition of 0.5 mM isopropyl-thiogalactoside (IPTG) for 16 hours at 25 °C. Pellets were resuspended in lysis buffer (300 mM NaCl, 20 mM HEPES, pH 8.0) and lysed with two passes through an Avestin emulsiflex C5 (Avestin) at 200 kPa of pressure. The lysate was clarified by centrifugation (75000 g, 45 minutes, Avanti JXN26 centrifuge and JA25.50 rotor, Beckman Coulter) and applied with a peristaltic pump (flow 2 ml/min) to 10 ml of chelating sepharose resin (GE healthcare) preloaded with Ni2+, pre-equilibrated in lysis buffer and packed in an HK-16/30 column holder (GE healthcare). The column was then washed with 1M NaCl, 20 mM HEPES pH 8.2, transferred to an AKTA or DuoLogic Bioflow liquid chromatography system (GE healthcare / Biorad, respectively), washed further with 300 mM NaCl, 50 mM imidazole pH 8.0, 20 mM HEPES pH 8.0?. The protein was eluted using gel filtration buffer (100 mM NaCl, 20 mM HEPES pH 8.2) supplemented with 250 mM imidazole pH 8.0, dialysed overnight against gel filtration buffer + 5 mM dithiothreitol (DTT), concentrated by ultrafiltration (Amicon ultra, 3000 MWCO) and further purified by size exclusion chromatography (Superdex 75 16/60, GE healthcare or ENrich SEC 70 10/300, Biorad). The resulting pure protein was concentrated, aliquoted, flash frozen and stored at -80°C. All steps after lysis were carried out at 4°C or on ice.

UCHL3 C95A, C95S

C95A and C95S mutants of His-SUMO-UCHL3 were generated by Quikchange site-directed mutagenesis (Agilent). Expression, lysis and affinity purification were carried out as for His-SUMO-UCHL3, but during dialysis, the SUMO-His tag was cleaved by digestion with SENP2 protease (NKI protein facility). UCHL3 was separated from the cleaved tag using a 10 ml nickel column, with UCHL3 collected from the flowthrough. The protein was then further gel filtered as detailed in His-SUMO-UCHL3.

UCHL3:$^{K27}Ub_2$ Complex

To obtain the UCHL3: $^{K27}Ub_2$ complex, UCHL3 and $^{K27}Ub_2$ were mixed in 1 to 1.1 ratio and incubated for 10' on ice; the excess of ubiquitin was removed by size exclusion chromatography (Superdex 75 10/300, GE healthcare) in 100 mM NaCl, 20 mM HEPES pH 8.1, and the protein complex was concentrated to 17 mg/ml by ultrafiltration after addition of 5 mM tris(2-carboxyethyl)phosphine (TCEP).

Biotinylated UCHL3 C95A

The biotinylated UCHL3 C95A-AviTag, used as anti-$^{K27}Ub_2$ western blotting reagent (Figure 1D), was obtained by fusing the AviTag sequence GLNDIFEAQKIEWHE (Daiss et al., n.d.) directly after the UCHL3 gene. Expression was performed as described for wild type UCHL3, but the bacterial pellet was resuspended in biotinylation buffer I (25 mM Hepes pH 8.3, 10 mM $Mg(OAc)_2$, 10 mM $CaCl_2$, 50 μM PMSF (Sigma), 15 μg/mL DNase I). The pellet was lysed by sonication, after which 10 mM ATP and 1 mM biotin were added to the suspension. Biotinylation was performed in total lysate with 50 μg/mL BirA ligase for 4 hours at 30 °C. The biotinylated UCHL3 C95A-AviTag protein was further purified as described above for wild type UCHL3.

Protein Ubiquitination

Ubiquitinated PCNA was produced according to the protocol described in (Hibbert and Sixma, 2012). Briefly, human PCNA was expressed and purified from *E. coli*, then ubiquitinated using 100 nM E1 (UBA1), 30 μM mutant E2 (UBCH5C S22R) and wild type Ub, $^{K63}Ub_2$ or $^{K27}Ub_2$. The reaction was carried out at 25°C in 100 mM NaCl, 5 mM $MgCl_2$, 5 mM ATP, 50 mM malic acid MES Tris (MMT) buffer, pH 9. Reaction progression was monitored by SDS PAGE.

(di)Ubiquitinated 3xSUMO2ΔN was produced by mixing 65 μM 3xSUMO2ΔN with 0.5 μM UBA1 (E1), 0.5 μM UBE2W (E2), 0.5 μM RNF4 and 2 μM synthetic Ub or Ub_2 in ubiquitination buffer (100 mM NaCl, 20 mM HEPES pH 7.5, 5 mM ATP, 5 mM $MgCl_2$). The mixture was incubated for 3 hours at 37°C, aliquoted and stored at -80°C.

Deubiquitination Reactions

Ub-Rho, Ub-His, Ub-L40-Rho, Ub-SUMO2

20 μM (9 μl) of each substrate were mixed with a serial dilution of UCHL3 (45 μM → 45 pM, 2 μl) in deubiquitination buffer (NaCl 100 mM, 20 mM HEPES pH 7.5, 5 mM DTT) and incubated at 37°C in a PCR machine for the indicated time. Reactions were quenched with boiling SDS loading buffer and resolved by SDS PAGE. All reactions were pipetted with a multichannel pipet to minimize time errors. Rhodaminated substrate bands were revealed using UV light in a Chemidoc XRS+ imager (Biorad Inc.); non-rhodaminated substrates were stained with Coomassie blue. The black and white Chemidoc gel images were colorized to magenta and blue in Adobe Photoshop for visualization purposes.

Ub-PCNA

Ubiquitinated PCNA (10 μM final concentration) was mixed with either UCHL3 (45 μM final) or recombinant USP7 (Kim et al., 2019) (1 μM final) in deubiquitination buffer and incubated for the indicated times at 37°C in a PCR machine. At each time point, aliquots were taken, immediately boiled for 5' in SDS loading buffer, and analyzed by SDS PAGE.

Ub(n)-3xSUMO2ΔN

Similar amounts (~1 μg, assessed by SDS PAGE) of Ub 3xSUMO2ΔN, $^{K63}Ub_2$-SUMO2ΔN and $^{K27}Ub_2$-SUMO2ΔN were incubated with 22 μM UCHL3 in deubiquitination buffer for the indicated time at 37°C. The reaction was aliquoted at the indicated time points and resolved by SDS PAGE, followed by western blot against SUMO2 (anti-SUMO2, Life Technologies 51-9100).

Crystallization and Structure Solution

Sitting drop crystallization screens were set up in 96-well format using a Mosquito crystallization robot (TTP Labtech), with 100 + 100 nl (protein + precipitant) drops. Initial crystals (plates + needles) were observed in multiple conditions containing polyethyleneglycol (PEG) 3350 and PEG 2000 mono methyl ether (20-30% w/v concentration range), with 0.1 M 2,2-Bis(hydroxymethyl)-2,2′,2″-nitrilotriethanol (Bis-Tris) pH <6.0 as buffer and various potassium salts or ammonium sulphate (0.1-0.2 M range). After optimization, the best diffracting crystals grew in 21% PEG 3350, 0.15M KBr, 0.1M Bis-Tris pH 5.5 and were cryoprotected by stepwise addition of 30% ethylene glycol prior to data collection. Data were collected by the Massively Automated Sample Selection Integrated Facility (MASSIF-1) (Bowler et al., 2016) at beamline ID30A-1 of the European Synchrotron Radiation Facility (ESRF) at a wavelength of 0.966 nm. The data were indexed, integrated and merged using XDS (Kabsch, 2010) and Aimless (Evans and Murshudov, 2013) in spacegroup $P22_12_1$ to a maximum resolution of 2.1 Å. Phasing was done by molecular replacement using Phaser (McCoy et al., 2007) with ubiquitin (PDB: 1UBQ, Vijay-kumar et al., 1987) and apo-UCHL3 (PDB: 1UCH, Johnston et al., 1997) as search models, followed by cycles of manual building and refinement with Coot (Emsley et al., 2010) and REFMAC (Murshudov et al., 2011) within the CCP4 suite (Winn et al., 2011). The final model was polished using the latest version of PDB_REDO (https://pdb-redo.eu, Joosten et al., 2014). Data collection and refinement statistics are in Table S1. Coordinates of the model were deposited under PDB: 6QML. The difference density in Figure S2C was generated by molecular replacement of the final model (minus Gly75,76 of the proximal ubiquitin) into the original data. All structural figures were generated using CCP4MG (McNicholas et al., 2011), with aesthetic fog, blur or colorization effects optionally added in Adobe Photoshop (Adobe Inc.). Structural superposition and root mean square deviation (rmsd) were calculated using the secondary structure matching (SSM) method (Krissinel and Henrick, 2004) in CCP4MG.

SURFACE PLASMON RESONANCE

100 ± 10 responsive units (RUs) of N-terminally biotinylated $^{K27}Ub_2$, $^{K63}Ub_2$ or Ub were immobilized on lanes 2-4 of a single streptavidin chip (SA chip, GE healthcare). Increasing concentrations of wild type or mutant UCHL3 (range 60 pM - 65.5μM) or UCHL1 (60 pM - 35.5 μM) were flowed over the chip at a speed of 30 μl/min and binding levels to each ligand was compared to the empty lane 1. The buffer used was 100 mM NaCl, 20 mM HEPES pH 7.5, 5 mM DTT, 0.05% TWEEN-20, supplemented with 10 mg/ml bovine serum

albumine (Sigma Aldrich), 1 mg/ml CM-Dextran (Sigma Aldrich) to reduce aspecific interactions. To account for different sized analytes, response units (RUs) of all experiments were normalized dividing by $k = RU_{immob} * MW_{analyte} / MW_{ligand}$, where RU_{immob} are the units of analyte on chip, and $MW_{analyte}$ and MW_{ligand} are the molecular weight of analyte and ligand. Binding data were fitted with a one site specific binding model in GraphPad Prism 7.0 (www.graphpad.com). Binding affinities are reported as K_d ± standard error. Plots were generated in Graphpad Prism and adapted for illustration using Adobe Illustrator (Adobe Inc.).

Diubiquitin Inhibition Experiments

Ub-Rho Cleavage

UCHL3 (10 pM final concentration) was pre-incubated for 30 minutes at room temperature with diubiquitin (5 nM final concentration), monoubiquitin (10 nM final concentration), buffer (positive control) or iodoacetamide (negative control, 10 mM final concentration). Then, Ub-Rho (500 nM final concentration) was added and fluorescence intensity (λex = 487 - 14 nm, λem = 535 - 30 nm) was measured every 20 seconds for 60 minutes on a Clariostar (BMG Labtech) microplate reader. Each condition was measured in quadruplicate using a volume of 8 μl per well. Buffer conditions: 50 mM Tris (pH 7.6), 50 mM NaCl, 2 mM 1,4-Dithiothreitol (DTT), 0.05% Tween-20. The data were plotted using GraphPad Prism 7.

Ub-His Cleavage

Ub-His (100 μM final concentration), UCHL3 (50 nM) and either buffer (reference control) or the appropriate diubiquitin (0.5 μM) were mixed in 150 mM NaCl, 20 mM HEPES pH 8.1, 5 mM DTT. The reactions were incubated at 37°C and aliquots were taken at the indicated time points. The samples were resolved on a 4-20% Bolt gradient gel (Invitrogen) using MES-SDS running buffer and stained with Coomassie blue.

Ub-SUMO2 Cleavage

Reactions were performed as described above, in presence or absence of the appropriate diubiquitin (2.5, 5 or 10 μM). The sample was separated by SDS-PAGE and the bands were revealed by western blot. Antibodies: α-ubiquitin (mouse, 1:2000 (P4D1, Santa Cruz); α-SUMO2/3 (rabbit, Vertegaal et al., 2004 (Vertegaal et al., 2004)); donkey-α-rabbit IRDye®680 (LI-COR, cat. no. 926-68073); goat-α-mouse IRDye®800 (LI-COR, cat. no. 926-32210). Images were read out on an Odyssey Classic imager (LI-COR).

Stopped Flow Measurements

Equal amounts of a stock solution of ubiquitin substrate (100 nM for Ub-AMC, $^{K63}Ub_2$-AMC, $^{K27}Ub_2$-AMC; 50 nM for Ub-L40-Rho and $^{K27}Ub_2$-L40-Rho) and of UCHL3 (ranging in concentration from 0.025 to 128 nM) were mixed in a SF -61DX2 stopped flow fluorimeter system (TgK scientific Ltd, UK) with R10699 photomultipliers (Hamamatsu Photonics K.K., Japan). Measurements were carried out for 10s, with each measurement repeated 5 times and averaged for the final analysis. The plots of the stopped flow data and their residuals in Figures 5E, 5F, and S5 are displayed as percentage of response on the Y axis to facilitate visual comparison. Percentage of response was calculated by normalizing each dataset to the interval (0,100) using Graphpad Prism 7.0.

Kintek Modelling

Kintek Explorer version 8.0 (Kintek Corporation, Johnson et al., 2009a) was used to fit the reaction mechanism. Binding data from Figure 2B (Ub, $^{K63}Ub_2$, $^{K27}Ub_2$) and cleavage data from Figure 4B (Ub-AMC, $^{K63}Ub_2$-AMC, $^{K27}_{Ub2}$-AMC) were used for the fitting. The fitting presented here is based on all data, but the model was built in stages: first the cleavage data for Ub-AMC and $^{K63}Ub_2$-AMC was fitted to a product inhibition model (green part of model in Figure 6A and see text). In this model, k_{cut} and k_{-1} converged independently to very similar values (values $Ub_{(kcut)} = 47.8\ s^{-1}$; $Ub_{(k-1)} = 285\ s^{-1}$; $^{K63}Ub_{2(kcut)} = 49.5\ s^{-1}$; $^{K63}Ub_{2(k-1)} = 295\ s^{-1}$). The cleavage of $^{K27}Ub_2$-AMC was then considered. The simplest model that could account for the observed kinetics is the entire model in 6a (green + cyan paths). When fitting this model to $^{K27}Ub_2$-AMC cleavage, the k_{cut} converged to $38.8\ s^{-1}$, a value similar to that calculated for Ub-AMC and $^{K63}Ub_2$-AMC. We then fitted all three substrates (Ub-AMC, $^{K27}Ub_2$-AMC, $^{K63}Ub_2$-AMC) with the entire model in 6a. Given the independent convergence of k_{cut} an k_{-1} from the different substrates, we imposed the conditions: (1) Ub-AMC $_{(kcut)}$ = $^{K63}Ub_2$-AMC $_{(kcut)}$ = $^{K27}Ub_2$-AMC $_{(kcut)}$ and (2) Ub-AMC $_{(k-1)}$ = $^{K63}Ub_2$-AMC $_{(k-1)}$. Finally, we added the binding data for Ub, $^{K63}Ub_2$ to the final fit, leading to the values of the constants reported in Figures 6A, 6B, S6C, and S6D. Landscape analysis of the fitted parameters using FitSpace Editor (Johnson et al., 2009b) showed correlation between values of k_{open1} and k_{close1} and between k_{open2}, and k_{close2}. Thus, only their ratios and magnitude are directly defined within the model. The fitting residuals in Figure S6C were calculated as $FI_{observed}$ - $FI_{calculated}$. The plots in Figure S5D were calculated using FitSpace Editor of the Kintek software.

To estimate the probability of choice between the open and closed cleavage pathways, we used the general model to simulate the equilibrium ratio between the open and closed $^{K27}Ub_2$-AMC:UCHL3 complexes in conditions when the rate of $^{K27}Ub_2$-AMC cleavage was set to zero. Then we assumed: (1) $P_{open}/P_{close} = [^{K27}Ub_2\text{-AMC:UCHL3}]_{open}/[^{K27}Ub_2\text{-AMC:UCHL3}]_{closed}$ and (2) $P_{open} = 1 - P_{close}$, where P_{open} and P_{close} are the probabilities of open and closed cleavage, and $[^{K27}Ub_2\text{-AMC:UCHL3}]_{open}$ and $[^{K27}Ub_2\text{-AMC:UCHL3}]_{closed}$ are the concentration of the open and closed substrate:enzyme complex at equilibrium reported by the simulation. The probabilities derived with this method are essentially identical to those derived by looking at the ratio of k_{open1} and k_{close1} in the model. Standard error on the estimate was calculated using error propagation from the errors of the kinetic constants.

Detection of $^{K27}Ub_2$ with Biotinylated UCHL3

Equal amounts of mono and diubiquitin (500 ng) were run on a 4-12% Bis-Tris gel in MES buffer (NuPAGE, Life Technologies) and transferred to a 0.2 μm nitrocellulose membrane using a Trans-Blot Turbo transfer system (BioRad). The membrane was blocked for

30 minutes with 5% milk (skim milk powder, LP0031, OXOID) in 0.2% PBS-Tween20 (PBST) and incubated with primary α-ubiquitin (mouse monoclonal, 1:2000 (P4D1, Santa Cruz) antibody or biotinylated UCHL3 C95A-AviTag (0.1 μg/mL) for 1 hour at room temperature. After washing, three times 15 minutes in 0.2% PBST, the blot was incubated with the secondary antibody goat-anti-mouse IRDye®680 (LI-COR, cat. no. 926-68070) or neutravidin DyLight800 (Thermofisher Scientific, cat. no. 22853). Images were read out on an Odyssey Classic imager (LI-COR).

Experimental Design

Unless otherwise specified in the relevant section, all experiments were repeated at least two times with comparable results. No blinding was applied. Randomization of samples is not applicable.

QUANTIFICATION AND STATISTICAL ANALYSIS

Assumptions and procedure used for kinetic model fitting are discussed in Method Details, Kintek modeling. Residuals of modeitting and chi^2/chi^2 simulations are shown in Figures S5B–S5D and were calculated using FitSpace within the Kintek software suite.

SPR measurements treatment, normalization and fitting are discussed in Method Details, Surface Plasmon Resonance. Binding affinity fitting was performed in GraphPad Prism 7.0 using a single, specific binding model.

Data and model quality of the crystallographic structure are summarized in Table S1 and were calculated automatically by the appropriate software within the CCP4 suite. Extended data and model quality analysis were calculated by the Protein Data Bank upon deposition and can be found at the entry page (PDB id 6QML).